Non-equilibrium Ensembles for the 3D Navier-Stokes Equations

G. Margazoglou,[1,2,*] L. Biferale,[3] M. Cencini,[4,5] G. Gallavotti,[6] and V. Lucarini[1,2]

[1] *Department of Mathematics and Statistics, University of Reading, Reading, United Kingdom*
[2] *Centre for the Mathematics of Planet Earth, University of Reading, Reading, United Kingdom*
[3] *Department of Physics and INFN, University of Rome Tor Vergata, 00133 Rome, Italy*
[4] *Istituto dei Sistemi Complessi, CNR, via dei Taurini 19, I-00185 Rome, Italy*
[5] *INFN Rome Tor Vergata, Rome, Italy*
[6] *INFN Roma1 & Accademia dei Lincei, Rome, Italy*

(Dated: December 27, 2021)

At the molecular level fluid motions are, by first principles, described by time reversible laws. On the other hand, the coarse grained macroscopic evolution is suitably described by the Navier Stokes equations, which are inherently irreversible, due to the dissipation term. Here, a reversible version of 3D Navier Stokes is studied, by introducing a fluctuating viscosity constructed in such a way that enstrophy is conserved, along the lines of the paradigm of microcanonical versus canonical treatment in equilibrium statistical mechanics. Through systematic simulations we provide evidences of the conditions that must be satisfied in order to have a statistical equivalence between the two non-equilibrium ensembles. Moreover, we numerically study the empirical distribution of the fluctuating viscosity by changing the Reynolds number and the number of modes used in the discretization of the evolution equation.

PACS numbers: 47.10.ad Navier-Stokes equations; 47.27.E- Turbulence simulation and modeling; 05.40.-a Fluctuation phenomena, random processes, noise, and Brownian motion
Keywords: Equivalence Hypothesis, Reversibility, 3D Navier Stokes, Turbulence

I. INTRODUCTION

The statistical balance between energy injection and dissipation is the key ingredient for the establishment of steady state conditions in non-equilibrium statistical mechanical systems. Such systems are driven out of equilibrium by the presence of an external forcing, while dissipation acts as a thermostat that removes the excess of energy[1, 2], with entropy being produced in the process.

In the case of fluid systems, described by the Navier Stokes equation (NSE) [3, 4], dissipation is introduced in the form of a Laplacian operator acting on the velocity field times a positive constant - the viscosity. Such an operator preferentially damps the small scales of the flow. There are other ways to introduce dissipation, and two relevant examples are given next. For instance, in 2D and geophysical flows, dissipation is often introduced via the Ekman friction, which is justified e.g. by the effects of the bottom and top surfaces of the thin fluid layer which helps avoiding accumulation of energy at large scales[5, 6]. Another approach, used customarily in numerical simulations to reach high intensity turbulent states in many applications, is to introduce hyperviscosity [7], *i.e.* a positive power of the Laplacian, which confines dissipation to the small scales, acting, *de facto*, like a sharp ultraviolet filter. It is also possible to introduce dissipation by combining more than one of the above outlined approaches. The common characteristic among all the forms of dissipation described above is that they break the time reversal symmetry, which is instead preserved by the other terms of the NSE.

Reversible equations govern microscopic motion while irreversible equations describe, very often, macroscopic evolution of the same systems with equations derived via scaling of various parameters [8–11]. Thus the question arises as of whether the macroscopic description of systems evolving irreversibly could also be described macroscopically by reversible equations.

The equivalence of different ensembles in equilibrium statistical mechanics (see e.g. [12, 13]) describes, in the thermodynamic limit, the independence of macroscopic observables with respect to the chosen thermostat, which defines the underlying microscopic interactions between the system and the reservoir in contact with it. In non-equilibrium systems it is possible to appropriately modify the irreversible term(s) of the evolution equation in such a way that time reversibility is restored, while, under suitable constraints, a macroscopic quantity is kept fixed [14]; an early example for NSE is in [15] where many conditions are simultaneously imposed to constrain that the energy content obeys at every scale (above the Kolmogorov's) the 5/3 law. The key question is whether, and under which conditions, the two ensembles (irreversible and reversible) are equivalent and describe the same physical problem.

In the context of fluid systems, where the viscous term is the source of irreversibility, it is possible to introduce a velocity field-dependent fluctuating viscosity, such that the viscous term becomes formally reversible, while keeping fixed a macroscopic quantity (e.g. the energy or enstrophy, etc.) as a constraint. The equivalence between the irreversible and reversible fluid ensembles was first conjectured in [16, 17] in the limit of vanishing viscosity and fixed system size. Subsequent numerical attempts

* Corresponding author. Email: g.margazoglou@reading.ac.uk

addressed this conjecture in a few simple systems such as in a version of the 2D NSE truncated to a few modes and with periodic boundary conditions [18], and more recently in [2, 19], in the Lorenz-96 model [20] and a shell model of turbulence [21, 22]. Recently, an interesting attempt to show equivalence between a reversible 2D NSE, where both energy and enstrophy are kept fixed, with irreversible 2D NSE is presented in [23]. First in [24] and later in [2, 25, 26] a second conjecture was laid to address the equivalence in the limit of infinite system size at fixed viscosity.

Attempts to investigate the properties of the reversible ensemble for the 3D NSE have only very recently been made [27, 28]. In [27], where the fluctuating viscosity is constructed in such a way as to keep the energy at a constant value, the authors gave insight of a possible second order phase transition between the two statistically steady regimes that 3D NSE can exhibit, see Sec. III B, in the dual limit of infinite system size and vanishing viscosity, and gave a suggestion of the parametric space where the conjectures should be addressed. In [28], where enstrophy is kept constant, the authors employ high spatial resolutions at small viscosities and by comparing the expectation values of several different observables provide some evidences of the agreement between the generated ensembles of irreversible and reversible 3D NSE.

The goal of the present work is twofold. First, we wish to study the domain of validity of the two conjectures for the 3D NSE, by thoroughly investigating the distributions of several observables at different scales, with attention to expectation values and standard deviations. Second, we wish to study the statistics of the fluctuating viscosity in the statistically steady regimes, which provides insights for the conditions of smoothness of the velocity fields.

The paper is structured as follows. In Sec. II we present the necessary theory and state the Conjectures we wish to test in our study. In Sec. III the results of the numerical simulations are provided. The results pertaining the two Conjectures are separately addressed in Sec. III D and Sec. III E, respectively. In Sec. IV we discuss the results on the statistics of the fluctuating viscosity for the reversible NSE. We summarize our findings and provide some perspectives in Sec. V. We further supplement our work with a series of Appendices.

II. VISCOSITY AND REVERSIBILITY

A. Irreversible Navier-Stokes Equation in 3D

Here we consider the classical case of an incompressible fluid enclosed in a 3-dimensional container with periodic boundary conditions, described by the NSE. Assuming incompressibility amounts to removing internal energy from the energy content of the fluid.

The NSE can be written as

$$\partial_t \boldsymbol{u} = \nu \Delta \boldsymbol{u} - \boldsymbol{u} \cdot \boldsymbol{\partial}\, \boldsymbol{u} - \boldsymbol{\partial} p + \boldsymbol{f}, \tag{1}$$

where $\boldsymbol{u}(\boldsymbol{x}, t)$ is imposed to have zero divergence and zero spatial average, p is the pressure field, ν is the viscosity, and $\boldsymbol{f}$ is a force field. The NSE is fundamentally difficult in 3D because it is not known whether solutions could be constructed with sufficient generality. For instance, if we suppose that $\boldsymbol{f}$ acts only at large scales (*i.e.* confined to a finite number of modes) and the initial data have only a finite number of modes, then it is not known whether, in such a generality and no matter how small $\nu > 0$ is fixed, a smooth solution follows for all $t > 0$. Note that this formulation of the problem is slightly weaker than the millennium problem B of the Clay Mathematics Institute [29].

On the other hand, equally hard problems arise in statistical mechanics systems; for instance, in 3D there is no existence theorem for an infinite system of hard spheres starting at an initial state in which the maximal speed and the minimal particles distance in any unit box are bounded away from ∞ and 0. Notwithstanding, this has not been an obstacle for developing the statistical mechanical theory of phase transitions.

The obvious way forward is to introduce extra parameters which regularize the equations, turning them into equations which admit solutions and try to study only properties that can be shown to be independent of the regularization parameters. For instance, in the case of statistical mechanics the equations are typically regularized by confining the system to a finite box, say a cube of volume V.

In the present case we consider the truncated NSE, *i.e.* the regularized version of Eq. (1) in Fourier space obtained by requiring that $\boldsymbol{u}$ is periodic in the container and has only modes $\boldsymbol{k} = (k_1, k_2, k_3)$ with $k \leq N$, and $k \overset{def}{=} ||\boldsymbol{k}||_2 = \sqrt{k_1^2 + k_2^2 + k_3^2}$. We focus on properties of the solutions which hold uniformly in the cut-off N, and the container is supposed to be of size $[0, 2\pi]^3$. Therefore, one can introduce the complex scalars $u_{\beta,\boldsymbol{k}} = \overline{u}_{\beta,-\boldsymbol{k}}$, where the overline notation denotes the complex conjugate, and two unit vectors $\mathbf{e}_\beta(\boldsymbol{k}) = -\mathbf{e}_\beta(-\boldsymbol{k})$ mutually orthogonal and orthogonal to $\boldsymbol{k}$, so that the velocity field can be written as

$$\boldsymbol{u}(\boldsymbol{x}, t) = \sum_{\beta=1,2;\boldsymbol{k}} i\, u_{\beta,\boldsymbol{k}}(t)\, \mathbf{e}_\beta(\boldsymbol{k}) e^{-i\boldsymbol{k}\cdot\boldsymbol{x}}, \tag{2}$$

where the sum is restricted to $k \leq N$. Furthermore, by defining the kernel $T^{\beta_1,\beta_2,\beta}_{\boldsymbol{p},\boldsymbol{q},\boldsymbol{k}} = -(\boldsymbol{e}_{\beta_1}(\boldsymbol{p}) \cdot \boldsymbol{q})(\boldsymbol{e}_{\beta_2}(\boldsymbol{q}) \cdot \boldsymbol{e}_\beta(\boldsymbol{k}))$, and making the time notation implicit unless strictly necessary, the NSE can be expressed as

$$\partial_t u_{\beta,\boldsymbol{k}} = \sum_{\substack{\beta_1,\beta_2 \\ \boldsymbol{k}=\boldsymbol{p}+\boldsymbol{q}}} T^{\beta_1,\beta_2,\beta}_{\boldsymbol{p},\boldsymbol{q},\boldsymbol{k}}\, u_{\beta_1,\boldsymbol{p}} u_{\beta_2,\boldsymbol{q}} - \nu k^2 u_{\beta,\boldsymbol{k}} + f_{\beta,\boldsymbol{k}}, \tag{3}$$

with $k, p, q \leq N$. Due to the symmetry between $\boldsymbol{q}, \boldsymbol{k}$, the

sum over β_1, β_2 keeping $\boldsymbol{p}+\boldsymbol{q}+\boldsymbol{k}=\boldsymbol{0}$ yields the identity

$$\sum_{\beta_1,\beta_2} T^{\beta_1,\beta_2,\beta_2}_{\boldsymbol{p},\boldsymbol{q},\boldsymbol{k}}\, u_{\beta_1,\boldsymbol{p}} u_{\beta_2,\boldsymbol{q}} u_{\beta_2,\boldsymbol{k}} = 0, \tag{4}$$

reflecting the conservation of both the total energy, $\int d\boldsymbol{x}\, \boldsymbol{u}^2$, and the total helicity, $\int d\boldsymbol{x}\, \boldsymbol{u}\cdot(\boldsymbol{\partial}\wedge\boldsymbol{u})$ in the unforced and inviscid ($\nu=0, \boldsymbol{f}=\boldsymbol{0}$) limits.

B. Reversible Navier-Stokes Equation in 3D

Historically, discussions on the origin of dissipative macroscopic properties, out of purely reversible Newtonian dynamics at molecular level, go back at least to Maxwell (see Eq. (128) in [30]). Therefore, it is natural to expect that fluid motion can also be described by microscopic reversible equations. One can thus inquire whether even at the macroscopic level, although molecular motion is no longer explicitly playing a role, the same phenomena can be described by macroscopic reversible equations.

Here we shall study stationary states of the truncated NSE. The basic idea is that viscosity controls the regularity of the flow by forbidding uncontrolled growth of energy, and dissipates the input work by the forcing: $\int \boldsymbol{f}\cdot\boldsymbol{u}\, d\boldsymbol{x}$, proportionally to the product of viscosity times *enstrophy*

$$\nu\mathcal{D}(\boldsymbol{u}) = \nu\sum_{\boldsymbol{k},\beta} k^2 |u_{\beta,\boldsymbol{k}}|^2, \tag{5}$$

and where at steady state there is a statistical balance between input and output of energy. One can envisage that by replacing the viscous force $\nu\Delta\boldsymbol{u}$ with a reversible force that keeps the enstrophy constant many statistical properties of stationary states will remain correctly described, independently of the cut-off N [31].

The analogy with statistical mechanics is helpful; there, the cut-off is the volume of the container, and the equilibrium states can be described by different microscopic dynamics, like the energy conserving microcanonical distribution or the isokinetic evolution [14]. Both choices of states and evolution laws give the right statistics for *local observables*, *i.e.* observables depending on the configurations of particles located in a volume small compared to the total one, *i.e.* to the cut-off V. Most importantly, the statistical properties of such observables depend on V less and less as $V\to\infty$.

In the case of NS fluids subject to large scale forcing, locality is defined with respect to the Fourier space. The analogues of local observables are functions of the velocity field $\boldsymbol{u}$ that only depend on components $\boldsymbol{u_k}$ with k small compared to the cut-off N. More specifically, $O(\boldsymbol{u})$ is a local observable, when it depends only on a finite number of modes with $k<K$ for some $K<N$. This leads to the proposal that replacing the standard viscous force with a dissipative reversible term that keeps the enstrophy constant will lead to stationary states completely equivalent to the original dynamics up to an arbitrary K, as far as the statistical properties of local observables are concerned, provided N is large (ideally $N\to\infty$, in the same sense in which equilibrium thermodynamics becomes ensemble independent as the volume tends to infinity).

Specifically, we consider a new evolution equation where: (i) In Eq. (3) the external force $\boldsymbol{f}$ is fixed, with $||\boldsymbol{f}||_2 = const \in \mathbb{R}$, and acts on "large scale", *i.e.* it has finitely many modes: $\boldsymbol{f_k}=0$ if $k\geq k_f$ for some k_f. (ii) the viscous force $-\nu k^2\boldsymbol{u_k}$ is replaced by $-\alpha(\boldsymbol{u})k^2\boldsymbol{u_k}$, with $\alpha(\boldsymbol{u})$ defined such that the enstrophy

$$D = \mathcal{D}(\boldsymbol{u})$$

is a constant of motion. Note that a similar choice was followed by the authors in [28], while in [27] the kinetic energy was instead kept fixed. Such assumptions lead to the equations

$$\partial_t u_{\beta,\boldsymbol{k}} = \sum_{\substack{\beta_1,\beta_2\\ \boldsymbol{k}=\boldsymbol{p}+\boldsymbol{q}}} T^{\beta_1,\beta_2,\beta}_{\boldsymbol{p},\boldsymbol{q},\boldsymbol{k}}\; u_{\beta_1,\boldsymbol{p}}\, u_{\beta_2,\boldsymbol{q}} - \alpha(\boldsymbol{u})k^2 u_{\beta,\boldsymbol{k}} + f_{\beta,\boldsymbol{k}}, \tag{6}$$

where

$$\alpha(\boldsymbol{u}) = \frac{\Lambda(\boldsymbol{u}) + \sum_{\beta,\boldsymbol{k}} k^2 f_{\beta,\boldsymbol{k}}\overline{u}_{\beta,\boldsymbol{k}}}{\sum_{\beta,\boldsymbol{k}} \boldsymbol{k}^4 |u_{\beta,\boldsymbol{k}}|^2} = \frac{\Lambda(\boldsymbol{u}) + W(\boldsymbol{u})}{\Gamma(\boldsymbol{u})}, \tag{7}$$

with

$$\Lambda(\boldsymbol{u}) = \sum_{\substack{\beta_1,\beta_2\\ \boldsymbol{k}=\boldsymbol{p}+\boldsymbol{q}}} (T^{\beta_1,\beta_2,\beta_2}_{\boldsymbol{p},\boldsymbol{q},\boldsymbol{k}}\, k^2\, u_{\beta_1,\boldsymbol{p}} u_{\beta_2,\boldsymbol{q}} \overline{u}_{\beta_2,\boldsymbol{k}}) \tag{8}$$

obtained by multiplying both sides of Eq. (6) by $k^2\overline{u}_{\beta,\boldsymbol{k}}$, then summing over $\boldsymbol{k}$, and finally imposing that the r.h.s equals 0.

We call Eq. (3) Irreversible NSE (abbreviated as $\mathcal{I}$) and Eq. (6) Reversible NSE (abbreviated as $\mathcal{R}$). The name reversible refers to the property that if $S_t\boldsymbol{u}=\boldsymbol{u}(t)$ is a solution of $\mathcal{R}$, with initial data $\boldsymbol{u}_0$, and if $\mathcal{P}\boldsymbol{u}=-\boldsymbol{u}$, then $\mathcal{P}S_t\boldsymbol{u} = S_{-t}\mathcal{P}\boldsymbol{u}$ is also a solution, as a consequence of $\alpha(\mathcal{P}\boldsymbol{u}) = -\alpha(\boldsymbol{u})$. Instead, such an identity does not hold for the solutions of $\mathcal{I}$.

C. Conjectures

Let's introduce the collection $\mathcal{E}^{\mathcal{I},N}$ of the stationary distributions $\mu_\nu^{\mathcal{I},N}$ for the $\mathcal{I}$ evolutions, with cut-off N; for a given choice of $\boldsymbol{f}$ the distributions are parameterized by the Reynolds number $\mathrm{Re}\propto\nu^{-1}$. In principle, several distributions may correspond to the same Re although it is plausible that for Re large enough there is only one stationary distribution. Likewise let $\mathcal{E}^{\mathcal{R},N}$ be the collections of the stationary distributions $\mu_D^{\mathcal{R},N}$ for the $\mathcal{R}$ evolutions, with the same cut-off N. These are parameterized by the value D of the (constant) enstrophy. Again, in general, several distributions may correspond to the same D; similarly to the irreversible case,

it is plausible that for generic initial data and D large, $\mu_D^{R,N}$ is unique.

It is natural to associate to each distribution in $\mathcal{E}^{\mathcal{I},N}$ and $\mathcal{E}^{\mathcal{R},N}$ the average enstrophy $\langle\mathcal{D}(\boldsymbol{u})\rangle_\nu^{\mathcal{I},N}$ and, respectively, the enstrophy D, as well as the work per unit time dissipated:

$$\mathcal{W}_\nu^{\mathcal{I},N} = \int d\boldsymbol{x}\,\langle \boldsymbol{f}\cdot\boldsymbol{u}\rangle_\nu^{\mathcal{I},N}, \quad \mathcal{W}_D^{\mathcal{R},N} = \int d\boldsymbol{x}\langle \boldsymbol{f}\cdot\boldsymbol{u}\rangle_D^{\mathcal{R},N} \quad (9)$$

where $\langle O\rangle_\nu^{\mathcal{I},N}$, $\langle O\rangle_D^{\mathcal{R},N}$ denote the averages of an observable O over the distributions $\mu_\nu^{\mathcal{I},N}$ and $\mu_D^{\mathcal{R},N}$. Parameters ν, D at given N, will be said to be in correspondence if

$$\langle\mathcal{D}(\boldsymbol{u})\rangle_\nu^{\mathcal{I},N} = D. \quad (10)$$

In the present work, we perform a few preliminary checks, based on a numerical analysis of the truncated NSE, of the following two Conjectures on the distributions of local observables, originally presented in [1, 17, 18] respectively.

Conjecture 1: *If the parameters ν, D are in correspondence as described in Eq.* (10)*, then for all local observables $O(\boldsymbol{u})$ one has*

$$\frac{\lim_{\nu\to 0}\langle O\rangle_D^{\mathcal{R},N}}{\lim_{\nu\to 0}\langle O\rangle_\nu^{\mathcal{I},N}} = 1, \quad (11)$$

for all N.

Remark: In such cases where there are several invariant distributions with the same ν or same D, Eq. (11) has to be interpreted as implying that a correspondence can be set between a pair of distributions for each collection. Conjecture 1 was proposed and tested for different systems in a limited number of cases (*e.g.* [17, 20, 21]).

Introducing the *Kolmogorov scale* $k_\nu = \left(\frac{\varepsilon}{\nu^3}\right)^{1/4}$, with $\varepsilon = \nu\langle\mathcal{D}(\boldsymbol{u})\rangle$ being the energy dissipation rate, a different Conjecture is obtained in the limit when $N \to \infty$

Conjecture 2 – Equivalence Hypothesis: *Let O be a local observable, i.e. a function of $\boldsymbol{u}$ depending only on a finite number of modes with $k < K$. Then if $\mu_\nu^{\mathcal{I},N}$ and $\mu_D^{\mathcal{R},N}$ satisfy Eq. (10) one has*

$$\frac{\lim_{N\to\infty}\langle O\rangle_D^{\mathcal{R},N}}{\lim_{N\to\infty}\langle O\rangle_\nu^{\mathcal{I},N}} = 1 \quad (12)$$

for all ν and $K < c_\nu k_\nu$ with $0 < c_\nu \to c_0 \leq \infty$ as $\nu \to 0$.

Remarks:

1. Conjecture 1 relies on the chaoticity of the evolution at small ν and fixed N. Instead, Conjecture 2 concerns only the limit $N \to \infty$ and relies on the chaoticity of the microscopic motions leading to the NSE. Conjecture 2 is formulated for all ν, including the case where the asymptotic motion consists of periodic attracting sets. It just provides a quantitative version of Conjecture 1: given a local observable living on scale K the question of how small should ν be to achieve equivalence receives the quantitative answer that, in the limit $N \to \infty$, ν has to be such that $K < c_0 k_\nu$ which becomes eventually true, as lower and lower values of ν are considered, because k_ν diverges as $\nu \to 0$.

2. Conjecture 2 could be extended to more general macroscopic equations derived via scaling limits from microscopic reversible evolution.

3. In cases with more than one distribution for a given ν or D the interpretation should be that extra labels should be added to distinguish the various distributions and follow the remark in Conjecture 1. Conjecture 2 first appeared in [24] and was formally proposed in [25].

4. In [2, 26] a stronger Conjecture is directly formulated with $c_\nu = \infty$ for all ν. We will also test the validity of such a stronger version of Conjecture 2.

The two Conjectures differ in the order of consideration of the two limits, $\nu \to 0$ and $N \to \infty$. In particular, it is important to stress that the so-called fully developed turbulent limit is achieved in nature by $N \to \infty$ first and then $\nu \to 0$, *i.e.* it is captured by Conjecture 2. On the other hand, the limit $\nu \to 0$ for fixed N leads to a quasi-thermalization (in the sense of [32]) of the high wavenumbers range cut-offed by the maximum N. An additional feature of this regime is that the dimension of the attractor approaches the number of degrees of freedom of the system [20].

III. NUMERICAL SIMULATIONS

A. Setup

We have performed direct numerical simulations of both $\mathcal{I}$ and $\mathcal{R}$ equations for incompressible fluid in a triply periodic domain of size $L = 2\pi$. We used a dealiased (following the 2/3 rule [33]) parallel 3D pseudospectral code, based on the P3DFFT implementation [34], on cubic grids of size $N_0 = 64$, 128, 256, and 512 collocation points in each direction, effectively corresponding, via $N = N_0/3$, to $N = 21$, 42, 85, and 170 in Fourier space, respectively. N is the same as the cut-off scale k_{max} and will be used interchangeably. The time integration has been implemented with a second-order Adams-Bashforth scheme and a small timestep equal to $\Delta t = 10^{-4}$ was chosen for all the simulations; tests with different time steps have been done confirming that the one chosen was sufficient to ensure the robustness of the presented results. The grid size is $\Delta x = 2\pi/N_0$. The zero mode is not forced, ensuring that the mean velocity field remains zero at all times, and the external forcing

is deterministic and only acts on large scales, specifically in the $k_f \in [1, \sqrt{2}]$ domain. The phases were chosen as quenched random variables and kept equal in all simulations with $\sum_{\boldsymbol{k}} k^2 ||\boldsymbol{f}||_2^2 = 1$. We refer to Table I in Appendix C for a summary of the numerical simulations we performed, which are labeled as R#, where R stands for run in this context, followed by the number of the run, and a symbol, indicating the statistical regime each run belongs to; see discussion in Sec. III B.

We examine Conjectures 1 and 2 by testing a set of viscosities: $\nu = 5 \times 10^{-2}, 10^{-2}, 10^{-3}, 10^{-4}, 10^{-5}$ for different values of N. We proceed as follows. First we run a reasonably long $\mathcal{I}$ simulation at fixed ν, N and measure the average enstrophy $\langle D \rangle_\nu^{\mathcal{I},N}$ in the statistically steady state. Next, we start the $\mathcal{R}$ run from a steady $\mathcal{I}$ state for which the instantaneous enstrophy is $D = \langle D \rangle_\nu^{\mathcal{I},N}$. This step reduces the transient time required to reach the attracting set, but it is not strictly necessary, and in principle one can start from any initial condition with the appropriate enstrophy. We run the $\mathcal{R}$ for the same duration as the $\mathcal{I}$, and at each timestep we make tiny corrections by rescaling the velocity field as $\boldsymbol{u} \to \boldsymbol{u}\sqrt{\frac{\langle D \rangle_\nu^{\mathcal{I},N}}{D(t)}}$. Although, given the very small timestep we use, the deviations from condition (10) were tested to be small, the latter correction ensures that the total enstrophy stays constant within machine precision.

B. Statistically steady regimes

Two distinct statistically steady regimes can be identified for the $\mathcal{I}$ and $\mathcal{R}$ systems, depending on the cut-off N and Re (or, equivalently, on k_ν). One is what we call the *hydrodynamic* regime, achievable when N is large enough for any ν, such that $k_\nu \lesssim N$. It is characterized by a well developed inertial range (for small ν) with a $E(k) \sim k^{-5/3}$ scaling for $k_f \ll k \ll k_\nu$ and a well resolved exponential or superexponential decaying for large wavenumbers, where

$$E(k) = \sum_{\beta, k-\frac{1}{2}<k<k+\frac{1}{2}} \langle |u_{\beta,\boldsymbol{k}}|^2 \rangle \tag{13}$$

is the averaged spectral properties, or simply the energy spectrum. A scaling close to $E(k) \sim k^{-5/3}$ is observed in nature because of the regularising properties of viscosity at small scales [3, 4, 6]. The other, *-quasi-thermalized-* regime [32], features a $E(k) \sim k^2$ scaling for large values of k [32] and it is obtained at sufficiently small ν for any fixed N, such that $k_\nu \gg N$. We call this regime quasi-thermalized because the average energy content of the individual modes depends only weakly on k, given the geometrical degeneracy of the energy shells. A crossover region can be located between the two in the (N, ν) parameter space [27].

In Fig. 1 we present a first comparison between $\mathcal{I}$ and $\mathcal{R}$ by looking at $E(k)$ at changing ν and for fixed spatial resolution, $N_0 = 128$. Here, we have omitted in $\langle \cdot \rangle$ the

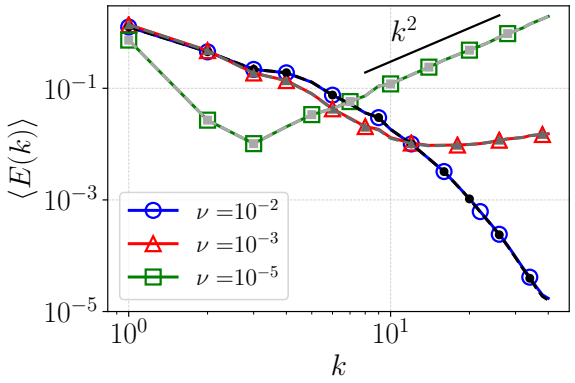

FIG. 1. Energy spectrum of $\mathcal{I}$ (grey-scale filled symbols) and $\mathcal{R}$ (colored open symbols) for $N_0 = 128$ and at changing ν (for $\mathcal{I}$) or D (for $\mathcal{R}$). We observe a well developed hydrodynamic regime for $\nu = 10^{-2}$ (R7◯), a crossover regime for $\nu = 10^{-3}$ (R8△) and a quasi-thermalized regime for $\nu = 10^{-5}$ (R10□); see Table I in Appendix C for details on the runs. (Color version online)

label $\mathcal{I}$ and $\mathcal{R}$ for simplicity and the same will be done in what follows whenever it does not lead to ambiguities. All regimes can be accessed as the viscosity is varied, and in terms of the average energy spectrum, the $\mathcal{I}$ and $\mathcal{R}$ agree remarkably well. This will be further checked in the following with respect to the two Conjectures. We anticipate that deviations will appear at scales k beyond the Kolmogorov scale k_ν, which will be further explored later. Next we will deal with the two regimes separately.

C. Mean properties of α

A rigorous -yet non trivial, see below- consequence of both Conjectures is the relation

$$\langle \alpha(\boldsymbol{u}) \rangle_D^{\mathcal{R},N} = \nu, \tag{14}$$

which holds when Eq. (10) holds. In Fig. 2(a) we validate Eq. (14). The errors are calculated by $\delta\mathcal{O} = \sigma(\mathcal{O})\sqrt{1 + 2\tau_\mathcal{O}}/\sqrt{j}$, where $\sigma(\mathcal{O})$ is the standard deviation, $\tau_\mathcal{O}$ the non-dimensional autocorrelation time, and j the ensemble size.

Figure 2(a) provides a consistency check, which looks at first not entirely obvious because α is not a local observable; see the definition given in Eq. 7. Yet, if the Conjectures and condition (10) hold, it must be true that the ensemble average of α is equal to the viscosity. This follows from the balance between energy input and output in steady state conditions that hold both for $\mathcal{I}$ and $\mathcal{R}$:

$$\begin{aligned} \nu \langle \mathcal{D}(\boldsymbol{u}) \rangle_\nu^{\mathcal{I},N} &= \langle \boldsymbol{f} \cdot \boldsymbol{u} \rangle, \qquad \mathcal{I} \\ D \langle \alpha(\boldsymbol{u}) \rangle_D^{\mathcal{R},N} &= \langle \boldsymbol{f} \cdot \boldsymbol{u} \rangle. \qquad \mathcal{R} \end{aligned} \tag{15}$$

Under the equivalence condition $\langle \mathcal{D}(\boldsymbol{u}) \rangle_\nu^{\mathcal{I},N} = D$, the value $\langle \boldsymbol{f} \cdot \boldsymbol{u} \rangle$ must be the same in $\mathcal{I}$ and $\mathcal{R}$, because $\boldsymbol{f} \cdot \boldsymbol{u}$

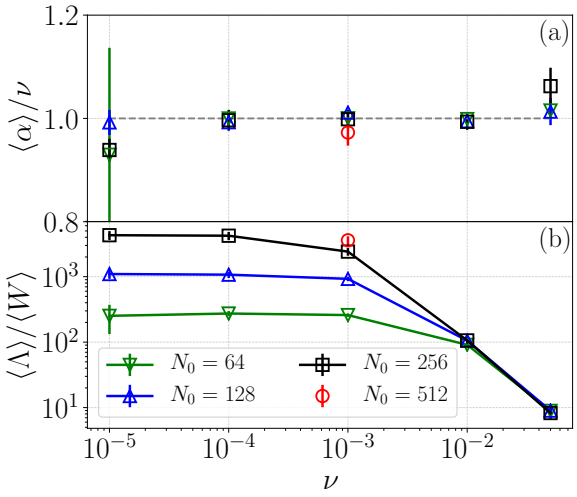

FIG. 2. Mean properties of α. (a) The ratio $\langle\alpha(\boldsymbol{u})\rangle_D^{\mathcal{R},N}/\nu = 1$ is a consistency check for equivalence conditions. (b) The ratio $\langle\Lambda\rangle/\langle W\rangle$ from Eq. (7) as a function of ν for all N_0 considered. The data are for $\mathcal{R}$. (Color version online)

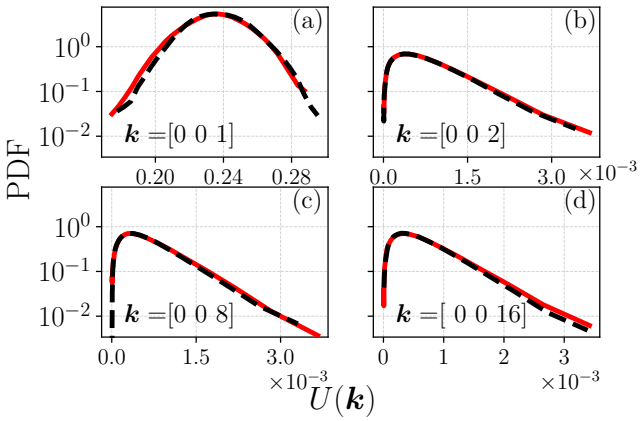

FIG. 3. Probability distribution function of single mode kinetic energy $U(\boldsymbol{k})$ for chosen modes $\boldsymbol{k} = (0, 0, m)$, $m = 1, 2, 8, 16$, showing the equivalence between $\mathcal{R}$ (red straight lines) and $\mathcal{I}$ (black dashed lines). Here $\nu = 10^{-4}$ and $N_0 = 64$ (R4□), belonging to the quasi-thermalized regime. (Color version online)

is a local observable. Hence, the relation $\langle\mathcal{D}(\boldsymbol{u})\rangle_\nu^{\mathcal{I},N} = D$ imposes the equality of the averages $\langle\boldsymbol{f}\cdot\boldsymbol{u}\rangle$ for the $\mathcal{I}$ and $\mathcal{R}$ systems, which, in turn, implies the *non trivial* relation (14). We remark that, as $\alpha(\boldsymbol{u})$ can be measured also in $\mathcal{I}$, we can also check its statistics. We observe that $\langle\alpha(\boldsymbol{u})\rangle_\nu^{\mathcal{I},N} = \nu$ in all statistical regimes, which is again non-trivial and a consequence of the equivalence conjectures even though α is not a local observable. Although the distributions of $\alpha(\boldsymbol{u})$ in both $\mathcal{R}$ and $\mathcal{I}$ are in all cases peaked around ν, as well as the mean values of both $\langle\alpha(\boldsymbol{u})\rangle_D^{\mathcal{R},N}$ and $\langle\alpha(\boldsymbol{u})\rangle_\nu^{\mathcal{I},N}$ are equal to ν, their tails are different in the hydrodynamic regime, but become almost identical in the quasi-thermalized regime (see Sec. IV B).

Since α is a sum of the forcing contribution $W(\boldsymbol{u})/\Gamma(\boldsymbol{u})$ and of the internal nonlinear contribution $\Lambda(\boldsymbol{u})/\Gamma(\boldsymbol{u})$ (8), it is interesting to remark that, on average, the non linear term dominates the forcing one as shown in Fig. 2(b), where the ratio $\langle\Lambda\rangle/\langle W\rangle$ versus ν is plotted. The ratio increases linearly as ν decreases in the hydrodynamic regime, before it approaches a (large) constant depending on N in the quasi-thermalized regime. Thus, on average the internal nonlinear exchanges dominate over the forcing for the $\mathcal{R}$ dynamics, introducing a non-local (in scale) coupling among all modes and making the validity of Conjecture 2 even less trivial.

D. Test of Conjecture 1 – Quasi-thermalized regime

In this section we address the validity of Conjecture 1 for 3D NSE. We remark that it has been confirmed in simpler dynamical systems in [18, 20–22]. Conjecture 1 applies when we consider decreasing values of ν at fixed N, which leads to the quasi-thermalized regime. In terms of observables, we consider the single mode kinetic energy, $U(\boldsymbol{k}) = ||\boldsymbol{u}(k_1, k_2, k_3)||_2^2$ and the energy spectrum, $E(k)$ (13) which will be presented separately.

1. *Single mode energy*

We consider the probability distribution function (PDF) of the energy $U(\boldsymbol{k})$ of a certain mode $\boldsymbol{k}$. In Fig. 3 we test this for a chosen type of modes, $\boldsymbol{k} = (0, 0, m)$, with $m = 1$, 2, 8, 16, and we see a very good agreement between the two ensembles, where the output of $\mathcal{R}$ is shown in red straight lines, while black dashed lines are used for the $\mathcal{I}$ simulations. In our analysis we have considered several different types of modes, i.e. permutations of $(0, 0, m)$, $(1, 0, m)$ and $(0, p, m)$, with $m = 1, \ldots, N$ and $p = 2$, or 7, or 9 (the latter integers were randomly chosen). The PDFs approximately follow a χ^2 distribution.

To further quantify the comparison between $\mathcal{I}$ and $\mathcal{R}$, we study the statistical properties of the ensembles of $U(\boldsymbol{k})$ by computing the mean $U^{(1)}(\boldsymbol{k}) \equiv \langle U(\boldsymbol{k})\rangle$, and the standard deviation $U^{(2)}(\boldsymbol{k}) \equiv \sqrt{\langle U^2(\boldsymbol{k})\rangle - \langle U(\boldsymbol{k})\rangle^2}$ of the timeseries for each measured mode $\boldsymbol{k}$. An indication of equivalence is when the ratios of such quantities are close to 1. In Fig. 4 we present the ratios of the mean $U_{\mathcal{R}}^{(1)}(\boldsymbol{k})/U_{\mathcal{I}}^{(1)}(\boldsymbol{k})$ (a) and the ratios of the standard deviation $U_{\mathcal{R}}^{(2)}(\boldsymbol{k})/U_{\mathcal{I}}^{(2)}(\boldsymbol{k})$ (b). To increase statistical accuracy, we further average the resulting ratios of the different types of modes considered here at each $m = 1, \ldots, N$, corresponding to the same shells k. As shown in Fig. 4, by fixing $N_0 = 64$ while decreasing ν, Conjecture 1 holds well in the case of single mode kinetic energy, which is a prototypical *local* observable, for the run (R4□). Note that the run (R3△) belongs to the

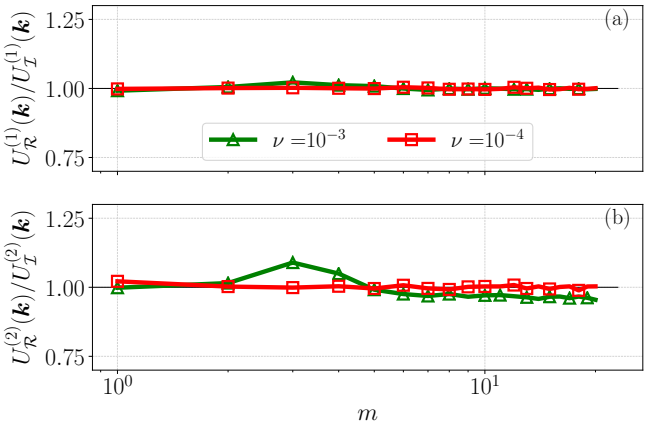

FIG. 4. Test of Conjecture 1 for single modes kinetic energy $U(\boldsymbol{k})$. (a) Averaged $\mathcal{R}/\mathcal{I}$ ratio of the mean of kinetic energy of considered modes, *i.e.* permutations of $(0, 0, m)$, $(1, 0, m)$ and $(0, p, m)$, with $m = 1, \ldots, N$ and $p = 2$, or 7, or 9. (b) Same for standard deviation ratio. The gray band indicates a 10% deviation from 1. Here $N_0 = 64$, and results from R3△, R4□ are shown. (Color version online)

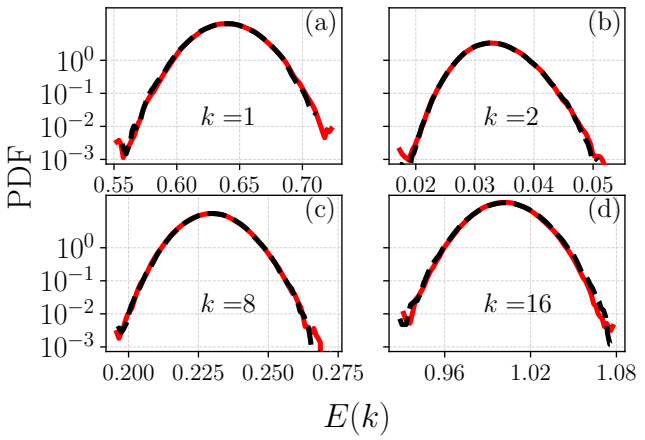

FIG. 5. Probability distribution function of energy spectra for $k = 1, 2, 8, 16$ showing the equivalence between $\mathcal{R}$ (red straight lines) and $\mathcal{I}$ (black dashed lines). Here $\nu = 10^{-4}$ and $N_0 = 64$ (R4□) corresponding to the quasi-thermalized regime. (Color version online)

crossover regime, hence outside the domain of validity of Conjecture 1, leading to some small deviations from 1 in Fig. 4(b). As a confidence interval, we introduce on qualitative grounds a 10% deviation from 1, displayed as a gray band.

2. *Energy Spectrum*

Subsequently, we study the energy spectrum, which has been briefly presented in Fig. 1. In Fig. 5 we show the PDF of kinetic energy for different shells $k = 1, 2, 8, 16$ for the case $N_0 = 64$ and $\nu = 10^{-4}$ (R4□). We notice that the statistics of $\mathcal{R}$ and $\mathcal{I}$ are almost identical and are approximately Gaussian as previously observed in [35]; deviation from Gaussianity are nonetheless present for $k = 2$.

In Fig. 6 we summarise the equivalence between the two ensembles by plotting the same of Fig. 4 but for the spectral properties at changing k and at fixed $N_0 = 64$. Accordingly, we define the mean $E^{(1)}(k) \equiv \langle E(k) \rangle$, and the standard deviation $E^{(2)}(k) \equiv \sqrt{\langle E^2(k) \rangle - \langle E(k) \rangle^2}$ of the timeseries for each shell k. As one can see, Conjecture 1 is well verified at decreasing ν and for any k. Notice in Fig. 6(b) that the standard deviation ratios for $\nu = 10^{-3}$ (green line-points) are different from 1 except for very small values of k. This is to be expected, as this case (R3△) belongs to the crossover regime, hence outside the domain of validity of Conjecture 1. Interestingly, for the same parameters, $\nu = 10^{-3}$, $N_0 = 64$, the single mode standard deviation ratios are close to 1; see the green line in Fig. 4(b). This reflects the higher complexity of the energy spectrum, resulting from the presence of correlations among Fourier modes. All the above confirm

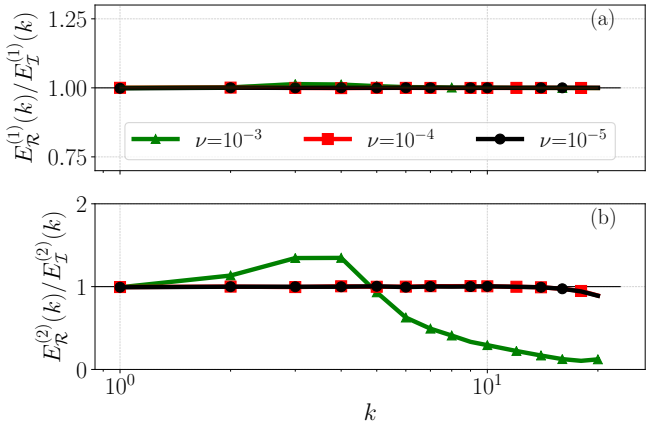

FIG. 6. Test of Conjecture 1 for the energy spectrum. (a) $\mathcal{R}/\mathcal{I}$ ratio of mean energy spectrum at shell k for $k = 1, \ldots, N$. (b) Same for standard deviation ratio. The gray band indicates a 10% deviation from 1. Here $N_0 = 64$, showing R3△ ($\nu = 10^{-3}$ - green triangles), R4□ ($\nu = 10^{-4}$ - red squares) and R5□ ($\nu = 10^{-5}$ - black circles). Note that we are here also inspecting the crossover regime (green triangles), hence outside the validity of Conjecture 1 (as shown in panel (b)). Nonetheless, good agreement is still found in panel (a). (Color version online)

the validity of Conjecture 1.

E. Test of Conjecture 2 – Hydrodynamic regime

We now present our numerical tests of Conjecture 2, which applies at fixed ν when N is large, corresponding to the hydrodynamic regime. Again, we consider the single mode kinetic energy and the energy spectrum.

1. Single mode energy

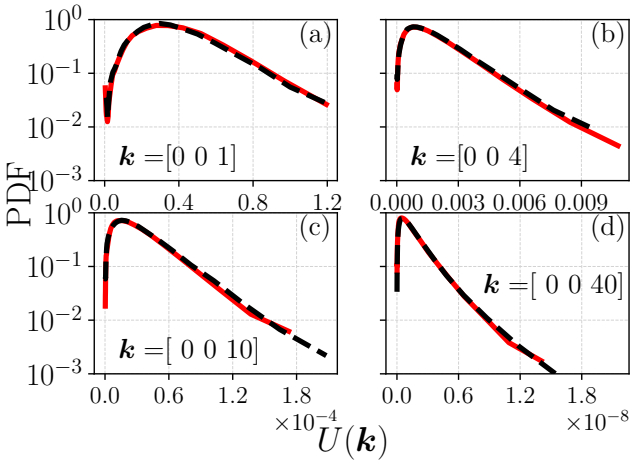

FIG. 7. Probability distribution function of single mode kinetic energy $U(\boldsymbol{k})$ for chosen modes $\boldsymbol{k} = (0, 0, m)$, $m = 1, 4, 10, 40$ showing the equivalence between $\mathcal{R}$ (red straight lines) and $\mathcal{I}$ (black dashed lines). Here $\nu = 10^{-2}$ and $N_0 = 128$ (R7◯), belonging to the hydrodynamic regime. (Color version online)

In Figure 7 we fix $N_0 = 128$, $\nu = 10^{-2}$ (R7◯) and compare the PDF of single mode kinetic energy, shifted to their mean, for the modes $\boldsymbol{k} = (0, 0, m)$, $m = 1, 4, 10, 40$ between $\mathcal{R}$ and $\mathcal{I}$. The agreement between the two ensembles is compelling.

A further analysis can be seen in Fig. 8 where all mean and standard deviation ratios of the timeseries have been collected for (a) $\nu = 10^{-2}$ and (b) $\nu = 10^{-3}$ for different values of N and m. In Fig. 8, for scales beyond the Kolmogorov scale k_ν (indicated by the red tick), we observe a disagreement between $\mathcal{R}$ and $\mathcal{I}$.

Therefore one could argue that, within the numerical set-up we have investigated in this work, k_ν is an approximate upper bound (in the sense of order of magnitude) for the maximum wavenumber K for which the Conjecture 2 applies; or as stated after Eq. (12), $c_\nu \approx 1$, both when considering $U^{(1)}(\boldsymbol{k})$, and $U^{(2)}(\boldsymbol{k})$. The observed difference between the $\mathcal{R}$ and $\mathcal{I}$ ensembles for $k \gtrsim k_\nu$ is further confirmed for all our well-resolved runs in the hydrodynamic regime. On the other hand, in the cross-over regime, *i.e.* here for R2◯ in Fig. 8(a) and R8△, R13△ in Fig. 8(b) the agreement for single mode statistics of the two ensembles, although not expected by Conjecture 2, is satisfactory.

2. Energy Spectrum

With respect to the energy spectrum at the hydrodynamic regime, we first present the distributions at low k. In Fig. 9 we plot the PDF of energy spectra at $k = 1$ and 3 for $\nu = 10^{-2}$ at $N_0 = 128$ (R7◯) and we observe a

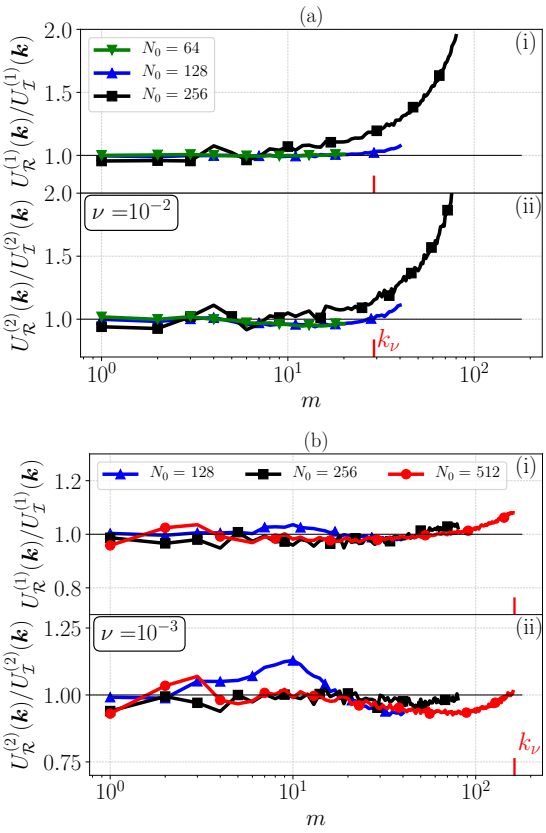

FIG. 8. Test of Conjecture 2 for single modes kinetic energy $U(\boldsymbol{k})$. (i) Averaged $\mathcal{R}/\mathcal{I}$ ratio of mean kinetic energy of considered modes and (ii) standard deviation ratio, at (a) $\nu = 10^{-2}$, and (b) $\nu = 10^{-3}$. The gray band indicates a 10% deviation from 1. The red vertical bar indicates the order of magnitude of the Kolmogorov scale, estimated as $k_\nu = \left(\frac{\varepsilon}{\nu^3}\right)^{1/4}$. (Color version online)

very good agreement between $\mathcal{R}$ (red line) and $\mathcal{I}$ (black dashed line). Then, in Fig. 10 the same are shown for a larger range of k, *i.e.* k =2, 4, 6, 20 and a smaller viscosity, $\nu = 10^{-3}$ at $N_0 = 512$ (R16◯), which is the only fully resolved run at $\nu = 10^{-3}$. Again, the agreement between the two ensembles is remarkable, and slight disagreement at the tails is likely due to statistical accuracy.

In Fig. 11 we collect the mean energy spectrum $E^{(1)}(k)$ at different k. We test the Conjecture 2 by quantifying the agreement between $\mathcal{R}$ and $\mathcal{I}$ through the ratio $E^{(1)}_{\mathcal{R}}(k)/E^{(1)}_{\mathcal{I}}(k)$, while fixing ν, at changing N. A deviation from 1 would indicate disagreement with respect to this observable. In Fig. 11(a) at $\nu = 10^{-2}$ we remark that $N_0 = 64$ (R3△) is slightly under-resolved (not well developed fall-off region in the spectrum), but still follows the same trend as the rest of the well resolved simulations at increasing k. Deviations occur for $k \gtrsim k_\nu$ when the ratio of $E^{(1)}(k)$ is considered. In Fig. 11(b) we show the results for $\nu = 10^{-3}$, where for all cases the ratio is close to 1 up until $k \sim k_\nu$, which is close to the cut-off of $N_0 = 512$. Also in (b), the ratio $E^{(1)}_{\mathcal{R}}(k)/E^{(1)}_{\mathcal{I}}(k)$ of

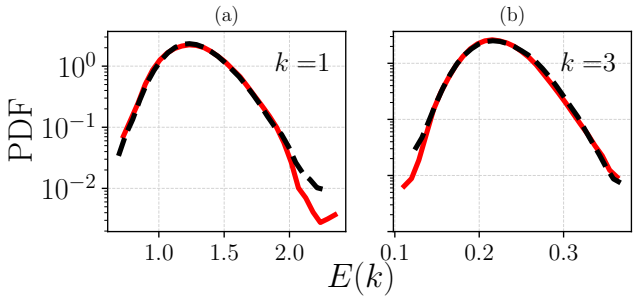

FIG. 9. Probability distribution function of energy spectrum showing equivalence between $\mathcal{R}$ (red straight lines) and $\mathcal{I}$ (dashed black lines), for $k = 1$, 3. For (a-b) it holds $E^{(1)}_{\mathcal{R}}(k)/E^{(1)}_{\mathcal{I}}(k) \approx 1$, and $E^{(2)}_{\mathcal{R}}(k)/E^{(2)}_{\mathcal{I}}(k) \approx 1$, confirming full equivalence between $\mathcal{R}$ and $\mathcal{I}$ up to $k \sim 4$ with respect to $E(k)$ at $\nu = 10^{-2}$ Here $\nu = 10^{-2}$ and $N_0 = 128$ (R7◯) corresponding to the hydrodynamic regime, and the y axis is in logarithmic scale. (Color version online)

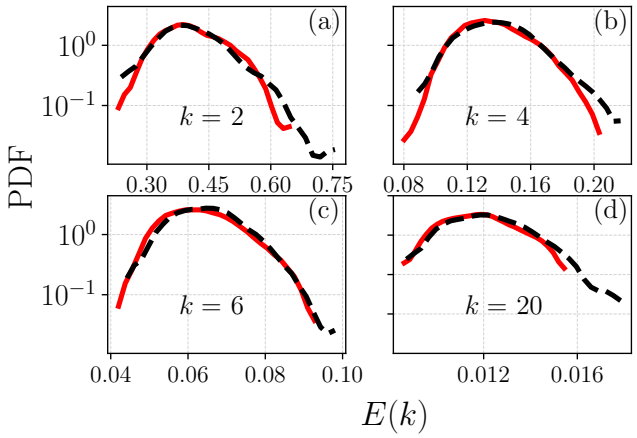

FIG. 10. Probability distribution function of energy spectrum showing equivalence between $\mathcal{R}$ (red straight lines) and $\mathcal{I}$ (dashed black lines), for $k = 2$, 4, 6, 20. For (a-d) it holds $E^{(1)}_{\mathcal{R}}(k)/E^{(1)}_{\mathcal{I}}(k) \approx 1$, and $E^{(2)}_{\mathcal{R}}(k)/E^{(2)}_{\mathcal{I}}(k) \approx 1$, confirming full equivalence between $\mathcal{R}$ and $\mathcal{I}$ up to $k \sim 20$ with respect to $E(k)$ at $\nu = 10^{-3}$. Here $N_0 = 512$ and $\nu = 10^{-3}$ (R16◯) corresponding to the hydrodynamic regime, and the y axis is in logarithmic scale. (Color version online)

the under-resolved runs ($N_0 = 128$ and $N_0 = 256$) stays unity for all k.

3. *Empirical determination of the locality cutoff K*

So far, the cases we have studied reveal a very good agreement between $\mathcal{R}$ and $\mathcal{I}$ for the quasi-thermalized regime (see Sec. III D), which confirms Conjecture 1, and full agreement for the hydrodynamic regime for $k \lesssim k_\nu$ when considering $U^{(1)}(\boldsymbol{k})$, $U^{(2)}(\boldsymbol{k})$, and $E^{(1)}(k)$. In accordance with the definition of Conjecture 2, we recall that a scale K can be defined such that observables depending on $\boldsymbol{u_k}$ with $k < K$ can be considered "local", thus determining the domain of validity of Conjecture 2. Furthermore, Conjecture 2 states that $K < c_\nu k_\nu$ with $0 < c_\nu \to c_0 \leq \infty$ as $\nu \to 0$. We state now that c_ν and accordingly K, can differ when considering different observables for testing the Equivalence. Indeed, for $U^{(1)}(\boldsymbol{k})$, $U^{(2)}(\boldsymbol{k})$, and $E^{(1)}(k)$ we concluded that $c_\nu \sim 1$.

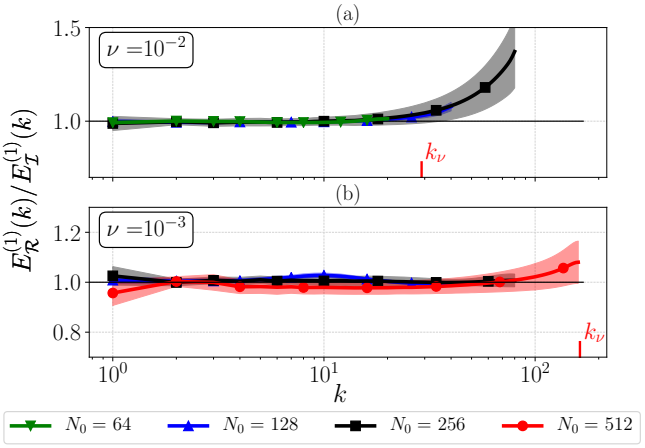

FIG. 11. Test of Conjecture 2 for the energy spectrum, considering the $\mathcal{R}/\mathcal{I}$ ratio of its mean at shell k for $k = 1, \ldots, N$, at (a) $\nu = 10^{-2}$, and (b) $\nu = 10^{-3}$. The transparent region corresponds to the statistical error. The gray band indicates a 10% deviation from 1. k_ν shows the location of the Kolmogorov scale. The plots share the same x-axis. (Color version online)

Next, we look at the statistics of energy spectrum at larger k. In Fig. 12 we show two examples where disagreement is observed in the case of $\nu = 10^{-2}$. Taking $N_0 = 256$ (R12◯) we show in (a) the PDF of $E(k)$ at $k = 10$, for which the ratios $E^{(1)}_{\mathcal{R}}(k)/E^{(1)}_{\mathcal{I}}(k) \approx 1$ (see Fig. 11 (a)), but $E^{(2)}_{\mathcal{R}}(k)/E^{(2)}_{\mathcal{I}}(k) \neq 1$. In (b) we choose a k larger than the Kolmogorov scale, *i.e.*

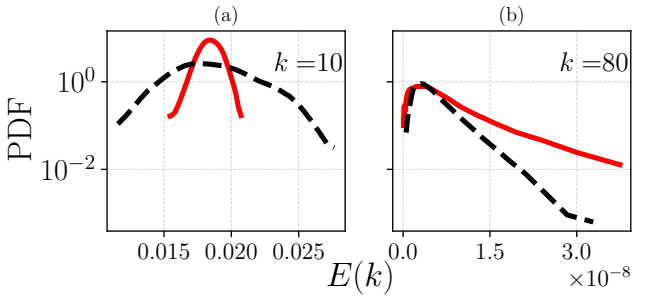

FIG. 12. Probability distribution function of energy spectrum for $\mathcal{R}$ (red straight lines) and $\mathcal{I}$ (dashed black lines) ($k = 10$ and $80 > k_\nu \sim 29$). For $k = 10$ the two distributions have the same mean. Here $\nu = 10^{-2}$ and $N_0 = 256$ (R12◯) corresponding to the hydrodynamic regime, and the y axis is in logarithmic scale. (Color version online)

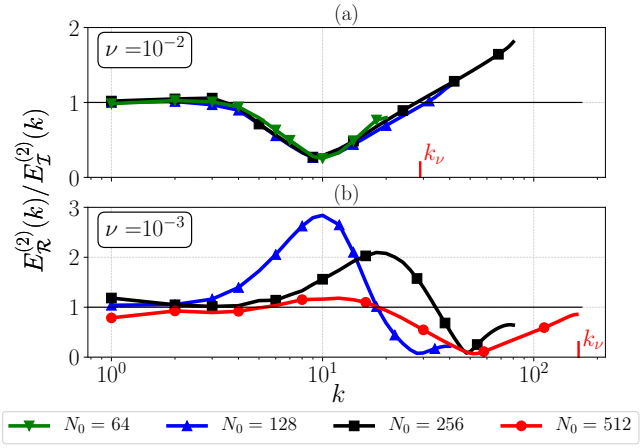

FIG. 13. Test of Conjecture 2 for the energy spectrum, considering the $\mathcal{R}/\mathcal{I}$ ratio of its standard deviation at shell k for $k = 1, \ldots, N$, at (a) $\nu = 10^{-2}$, and (b) $\nu = 10^{-3}$. In (a) the runs with $N_0 = 128$ and $N_0 = 256$ are fully resolved and belong to the hydrodynamic regime, while in (b) only $N_0 = 512$ is fully resolved. The gray band indicates a 10% deviation from 1. k_ν shows the location of the Kolmogorov scale. The range of validity of Conjecture 2 increases as we decrease viscosity in the hydrodynamic regime, as expected. The plots share the same x-axis. (Color version online)

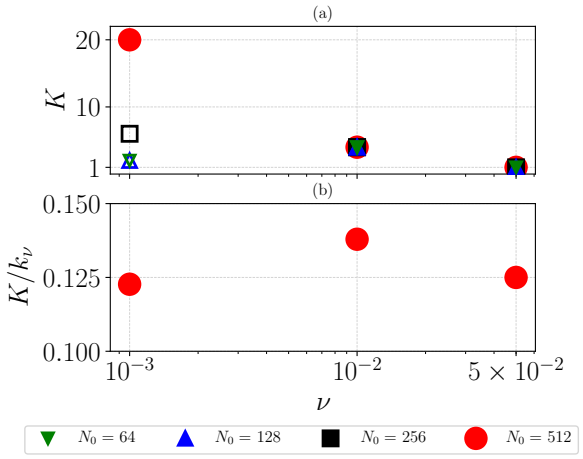

FIG. 14. (a) A quantitative estimate of the locality cut-off scale K, defined as the maximum wavenumber where all observables used to check the equivalence (Conjecture 2) have the same value within 10%, versus ν at different N_0. Here filled points correspond to runs in the hydrodynamic regime and open points to the crossover regime. (b) The ratio $c_\nu = K/k_\nu$ for all runs in the hydrodynamic regime as a function of ν, which is approximately constant. Both plots share the same x-axis in log scale. (Color version online)

$k = 80 > k_\nu \sim 29$, and both ratios of mean and standard deviation between $\mathcal{R}$ and $\mathcal{I}$ are not equal to 1.

In Fig. 13 we quantify the behavior of the standard deviation $E^{(2)}(k)$ of each ensemble, by considering their ratio $\mathcal{R}/\mathcal{I}$ for all k. Conjecture 2 is tested for fixed ν, (a) $\nu = 10^{-2}$ and (b) $\nu = 10^{-3}$ at increasing N. Starting from $k = 1$ there is initially agreement between $\mathcal{R}$ and $\mathcal{I}$ but we observe that $E^{(2)}_{\mathcal{R}}(k)/E^{(2)}_{\mathcal{I}}(k)$ departs from unity at a smaller k than $E^{(1)}_{\mathcal{R}}(k)/E^{(1)}_{\mathcal{I}}(k)$, which is also smaller than k_ν. Notice that in (a) the runs with $N_0 = 128$ and $N_0 = 256$ are fully resolved and belong to the hydrodynamic regime, and although the runs at $N_0 = 64$ are slightly under-resolved, it follows the same trend with the rest. Moreover, once the cut-off N is larger than k_ν by a sufficient margin, further increases in N do not change the features of the ratio curves, both for $E^{(1)}_{\mathcal{R}}(k)/E^{(1)}_{\mathcal{I}}(k)$ and $E^{(2)}_{\mathcal{R}}(k)/E^{(2)}_{\mathcal{I}}(k)$. Instead, in (b) only the $N_0 = 512$ case is fully resolved, and although $E^{(1)}_{\mathcal{R}}(k)/E^{(1)}_{\mathcal{I}}(k) \approx 1$ for all N_0 (see Fig. 11(b)) the standard deviation ratios differ when changing N_0. This occurs because $N_0 = 128$ and $N_0 = 256$ are under-resolved at $\nu = 10^{-3}$, and belong to the crossover regime (hence outside the validity of Conjecture 2), but are still displayed to show the transition from crossover to hydrodynamic regime, and how the agreement improves in that case.

To be more specific about the deviation from 1 with respect to Fig. 13, for (a) at $\nu = 10^{-2}$ it appears that $K \approx 4$. Instead, from Fig. 13(b) at $\nu = 10^{-3}$ it appears $K \approx 20$. The fact that K increases at decreasing ν, with sufficiently large N, is foreseen by Conjecture 2, and confirmed here. In other words, equivalence between $\mathcal{R}$ and $\mathcal{I}$ holds for a larger range of k, when the testing criterion is the shape of the distributions of $E(k)$, or similarly the standard deviation of it $E^{(2)}$.

The resulting values of K as extracted from second order moments of the energy spectrum, $E^{(2)}(k)$, are gathered in Fig. 14(a) for runs in the mixed hydrodynamic-crossover regime. Both at $\nu = 5 \times 10^{-2}$ and $\nu = 10^{-2}$ the runs are in the hydrodynamic regime, while at $\nu = 10^{-3}$ only $N_0 = 512$ (R16◯) is well resolved, for which we notice that K is maximum. In Fig. 14(b) we show that the empirically determined K does scale proportionally to k_ν, indicating that the range of scales where Conjecture 2 holds is increasing with the Reynolds number, i.e. supporting the statements that Conjecture 2 is uniformly valid in a sub-set of the inertial range for all turbulent intensities.

From Figs. 7-12, as well as Fig. 14(b), and with reference to Conjecture 2 it appears that within the case studied here we have:

- $c_\nu \sim 1$ when considering $U^{(1)}(\boldsymbol{k})$, $U^{(2)}(\boldsymbol{k})$, and $E^{(1)}(k)$ for the Equivalence test, and
- $c_\nu \sim 1/8$ when considering $E^{(2)}(k)$.

All the above confirm the validity of Conjecture 2 up to some wavenumber K.

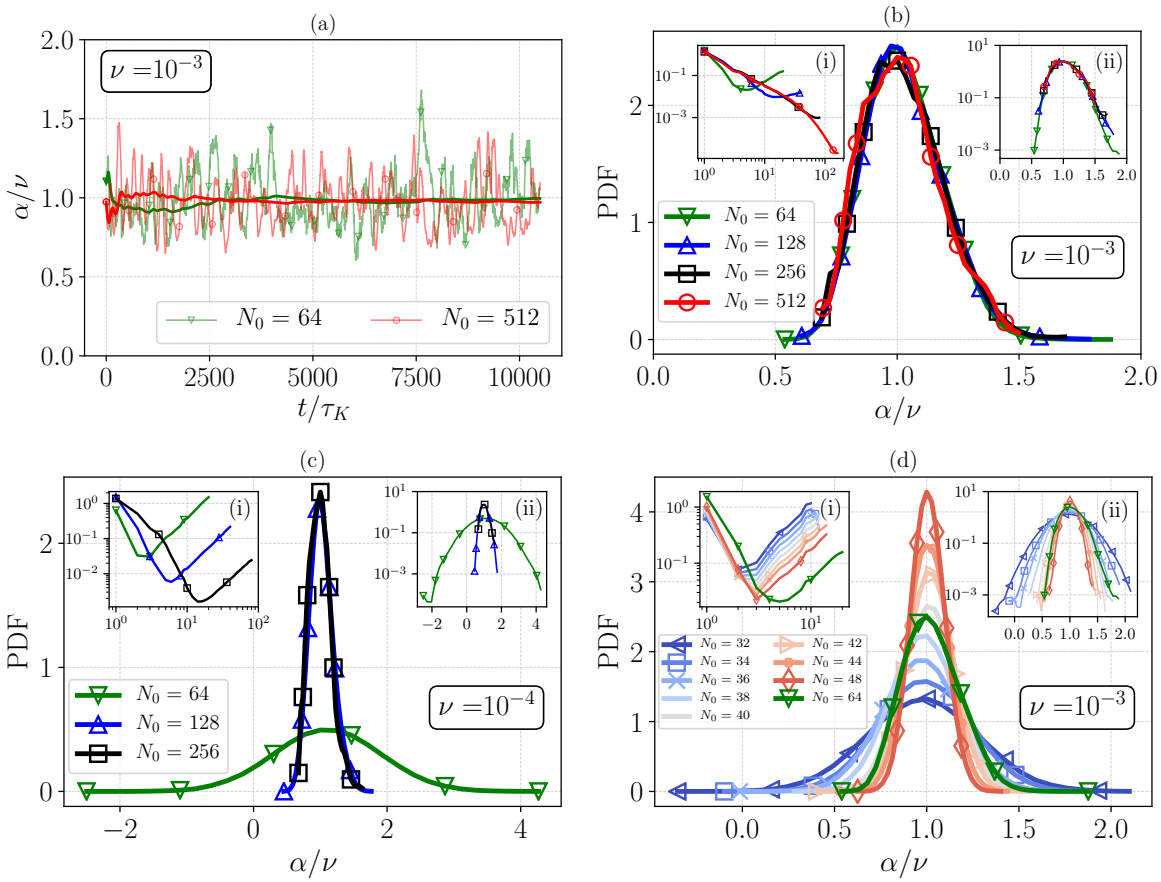

FIG. 15. Statistics of α for $\mathcal{R}$. (a) Temporal evolution of α/ν as a function of time, which is rescaled by the Kolmogorov time scale τ_K, at $\nu = 10^{-3}$. In solid line, green (for $N_0 = 64$) and red (for $N_0 = 512$) is the running average of α/ν. The fact that $\langle \alpha/\nu \rangle = 1$ in $\mathcal{R}$ is a rigorous prediction of Conjecture 2 (see also Eq. (14). (b) PDF of α/ν obtained considering the whole available statistics for each N_0, at $\nu = 10^{-3}$. The inset (i) is the energy spectrum, and inset (ii) is the PDF in log-scale. (c) Same as (b) at $\nu = 10^{-4}$. (d) Same as (b) at $\nu = 10^{-3}$ showing successively small N_0 between 32 and 64. (Color version online)

IV. PROPERTIES OF THE REVERSIBLE NAVIER STOKES EQUATIONS

For $\mathcal{R}$ the property that $\mathcal{D}(\boldsymbol{u})$ is a finite non-zero constant of motion has obvious implications on the sequence of solutions $\boldsymbol{u}^N(t)$ and for the Leray's solutions [36, 37], which are their weak limits as $N \to \infty$. Perhaps the most remarkable is an *a priori* upper bound on $\alpha(\boldsymbol{u})$ which can be proven (see Appendix A) to satisfy, for any solution and any N the condition:

$$|\alpha(\boldsymbol{u})| < C_2 \left(\sqrt{D} + \sqrt{D}^{-1} \right). \tag{16}$$

A second interesting and potentially very important remark on the $\mathcal{R}$ evolution is that *if* for all N large enough there were $\varepsilon > 0$ such that also: $0 < \varepsilon < \alpha < \kappa$, with probability 1 in the stationary state, then, it is possible to conclude that the attractor consists of $\boldsymbol{u}^N(t)$ with derivatives of all orders bounded uniformly in N, *i.e.* on the attractor the fields are uniformly smooth. This is an immediate consequence of the autoregularization results, see proposition 5, Sec. 3.2, in [38], and [39], and of the constancy of the enstrophy D, as shown in the Appendix B. Positivity of the lower bound on α is expected at large viscosity *i.e.* small Re.

Note also that by combining the aforementioned bound of Eq. (16), as proposed in the literature, with the fact that the dissipation νD in $\mathcal{I}$ has a positive limit as $\nu \to 0$ should indicate, (see [40, p.306]), that the upper bound on α is $O(\nu^{-\frac{1}{2}})$, which puts a limit to the fluctuations of α (which by the Conjecture is on average equal to ν; see also Sec. III C). Furthermore the upper bound (16) suggests that the transport contribution to α (*i.e.* $\Lambda(\boldsymbol{u})/\Gamma$) might dominate over the second term (*i.e.* the forcing contribution $(\int \Delta \boldsymbol{f} \cdot \boldsymbol{u})/\Gamma$), as confirmed in Fig. 2(b).

A. Numerical results about the sign of α in $\mathcal{R}$

In this section we inspect the statistics of the fluctuations of $\alpha(\boldsymbol{u})$ for $\mathcal{R}$, in order to assess the probability to observe negative values at varying the control param-

eters. In Fig. 15(a) we show in light colors the temporal evolution of α/ν, and in solid colors its running average, performed as $\frac{1}{t-t_0}\sum_{t'=t_0}^{t}\alpha(\boldsymbol{u}(t'))/\nu$ for $\mathcal{R}$ at $\nu = 10^{-3}$ and $N_0 = 64$, 512 (green - R3△ and red - R16◯, respectively). The presented time window, which is scaled by the Kolmogorov time $\tau_K = \sqrt{\nu/\varepsilon}$, is the maximum achieved for the run with $N_0 = 512$ (R16◯), while for R3△ this is only about 1% of its total temporal extend. Then, in Fig. 15(b) the PDFs of α/ν are presented for $N_0 = 64$, 128, 256, and 512 at $\nu = 10^{-3}$. Notably, all PDFs agree, even though at $\nu = 10^{-3}$ only $N_0 = 512$ is fully-resolved, belonging therefore to the hydrodynamic regime, while the other simulations belong to the crossover regime. The inset plots (i) and (ii) are respectively the energy spectrum and the PDF in semi-log scale.

In panel (c) we show the same of panel (b) but at lower viscosity, $\nu = 10^{-4}$, where the dataset at $N_0 = 64$ (R4□) is in the quasi-thermalized regime, while the other runs are in the crossover regime. As one can see, except for the case of the quasi-thermalized regime, in all other simulations we do not observe negative values of α within our statistical sample.

Additionally, in Fig. 15(d) we perform a detailed study at fixed $\nu = 10^{-3}$ and low resolution, in order to observe when, and how the transition to the occurrence of frequent negative values of α takes place. Starting from $N_0 = 64$ and gradually decreasing N_0, we observe that the PDF of α first turn from non-Gaussian to quasi-Gaussian, while becoming narrower (see $N_0 = 48$ and $N_0 = 44$), before starting to widen (see $N_0 = 40$ and $N_0 = 38$), until occurrence of $\alpha < 0$ events appears (see $N_0 \leq 36$). The rapid change in the left tail of the PDF at changing N_0 suggests that in order to further substantiate the asymptotic probability to observe negative α values, when N_0 is large and in the presence of intermediate or hydrodynamical regimes, one would need statistical samples significantly (exponentially) larger than those we could generate here, which is by far out of the scope of this paper and probably out of reach given the available computational power. This result is in agreement with some previous observations made in the context of a reduced model of turbulence [21].

In [28] negative values of α are observed in an $\mathcal{R}$ run at $N_0 = 1024$ and Taylor-based Reynolds number $\mathrm{Re}_\lambda = 300$. Certainly such results are somewhat puzzling and need to be explained/confirmed as we do not expect to be able to observe $\alpha < 0$ at such large N_0 and such Reynolds number, see subsection B below.

B. Numerical results about the sign of α in $\mathcal{I}$

Interestingly enough, $\alpha(\boldsymbol{u})$ is an observable that can be measured also in the $\mathcal{I}$ ensemble, by computing Eq. (7). In Fig. 16 we present the cases for two viscosities, $\nu = 10^{-2}$ (a-b) and $\nu = 10^{-3}$ (c-d). In (a), (c) we show the timeseries of $\alpha(\boldsymbol{u})/\nu$ for a time-window scaled by the Kolmogorov time scale τ_K, and in (b), (d) the corresponding PDF for different different resolutions N_0.

First, from panels (a)-(c) we note that also in $\mathcal{I}$ the non-trivial result $\langle\alpha(\boldsymbol{u})\rangle_\nu^{\mathcal{I},N} = \nu$ holds (see also Sec. III C). On the other hand, from panels (b)-(d) we observe some different behaviour from the corresponding PDF of the $\mathcal{R}$ ensemble in particular for the case of $\nu = 10^{-3}$. In the latter case the high wavenumber range starts to depart from the hydrodynamic regimes and probably have a direct impact on the fluctuations of α.

V. CONCLUSIONS

We present a detailed numerical study of 3D reversible Navier-Stokes equation (see Eq. (7)) obtained by imposing the conservation of enstrophy D via a thermostat, and compare our results with the output obtained from the corresponding (see Eq. (3)) standard irreversible NSE case. We investigate two Conjectures concerning the equivalence of the two ensembles. These Conjectures, which had been previously presented in [2, 26], pertain to two limiting conditions. The first equivalence is studied by keeping the flow evolving on a finite set of modes, and by decreasing the viscosity of the irreversible system or, equivalently, increasing the total enstrophy of the reversible one. In this limit, which leads to the regime that we have dubbed quasi-thermalized in the sense of [32], the equivalence between the two ensembles is more and more accurate with decreasing ν for any fixed N and for all scales, thereby confirming Conjecture 1.

The second Conjecture is studied in the physical regime where ν is held fixed and $N \to \infty$. In this case, there is a viscous cut-off, k_ν, separating the inertial range from the dissipative range in the irreversible system. We dubbed this regime hydrodynamic. In this regime we empirically observe that the equivalence between the two ensembles is restricted to "local" observables having support in a region of the Fourier space restricted by a typical wavenumber K, where K is smaller than -but proportional to- k_ν. This observation is consistent against changes in N and by decreasing the time discretization at least as far as we could test within our numerical capacities. The inertial-range equivalence between the two ensembles in the hydrodynamic limit is a further important confirmation of the robustness and universality of Navier-Stokes equations against changing of the dissipative mechanisms, at least concerning wavenumbers smaller than k_ν. This is particularly non-trivial as the dissipative term of $\mathcal{R}$ is highly nonlinear and non-local.

Note that, in Remark 4 of Sec. II C, we mentioned a stronger version of Conjecture 2, presented in [2, 26], where $c_\nu = \infty$ for all ν. Our results here make it appear doubtful that such Conjecture could hold in such a strong sense. However a study for a different fixed observable (instead of the enstrophy D), of the time scale, of the larger values N, and of the integration precision neces-

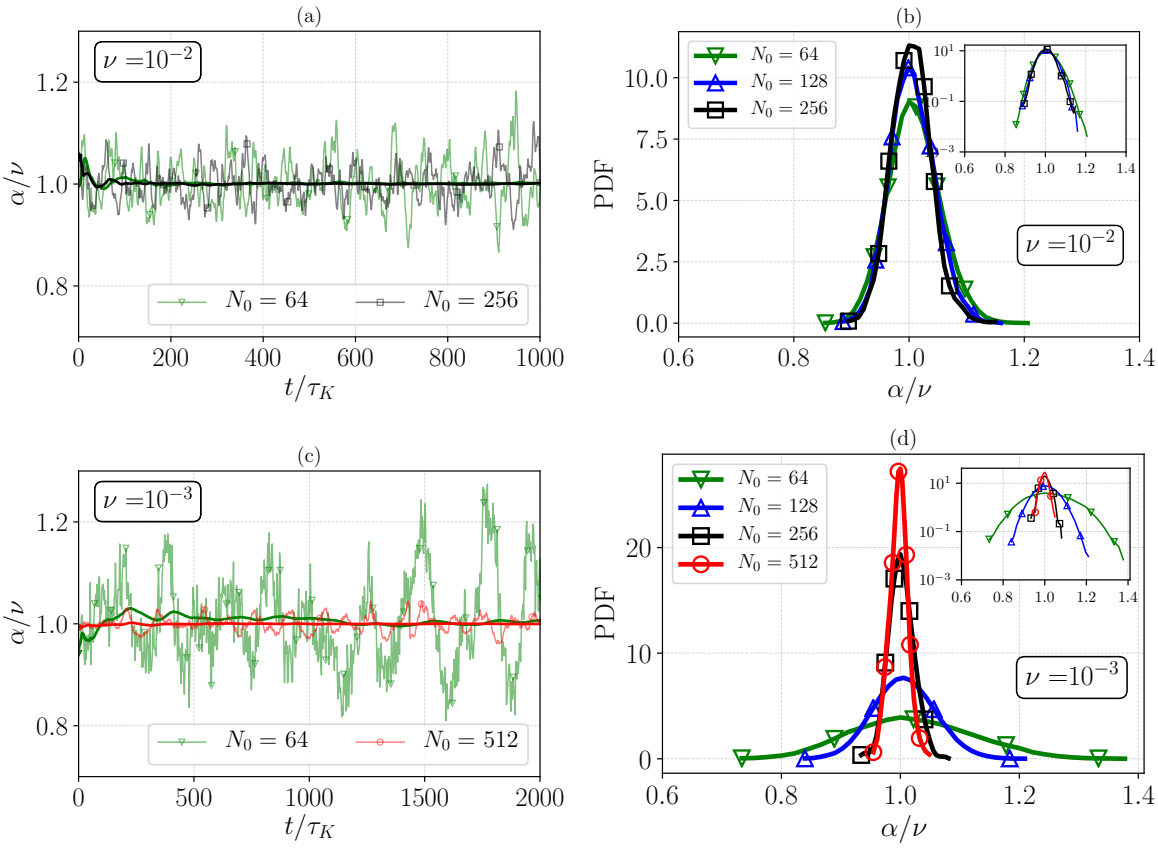

FIG. 16. Statistics of α for $\mathcal{I}$. (a), (c) Temporal evolution of α/ν as a function of time, which is rescaled by the Kolmogorov time scale τ_K, at (a) $\nu = 10^{-2}$ and (c) $\nu = 10^{-3}$. In solid line, green (for $N_0 = 64$) and red (for $N_0 = 512$) is the running average of α/ν. The fact that $\langle \alpha/\nu \rangle = 1$ within 0.1% in $\mathcal{I}$ is remarkable (in spite of the difference in fluctuations with $\mathcal{R}$), as α is a non-local observable, hence not directly expected by Conjecture 2. (b), (d) Probability Density Function of α/ν obtained considering the whole available statistics for each N_0, at (b) $\nu = 10^{-2}$ and (d) $\nu = 10^{-3}$. The inset is the PDF in log-scale. (Color version online)

sary to reveal the ν-dependence of c_ν, or even $c_\nu = \infty$ for all ν may be necessary to reach a firm conclusion.

Furthermore, we have presented a numerical empirical study of the PDF of the fluctuating viscosity for the reversible case, showing the existence of a trend towards less and less probable negative events by increasing the Reynolds in the hydrodynamical regime, similarly to what it has been observed in a reversible shell model [21]. The problem of the sign of α is related to that of the divergence of the phase-space contraction rate σ [26] and the problem of measuring the large deviations of σ is extremely delicate due to the fact that negative events are expected to happens with extremely small probability. We remark that, a recently published paper has presented results on the probability of observing negative values of α (see Fig. 4 of [28]) that are in contrast with what has been reported for the hydrodynamical limit ($N \to \infty$ first) in the present work. In particular, in [28] a transition in the shape of the PDF is observed for large numerical grids showing a non negligible probability to have negative events.

Finally, by studying the average of α for the $\mathcal{I}$, we have shown that equivalence can also hold non local observable, which is a non trivial application of the Conjectures. So, it would be natural to test whether equivalence might be extended to other important non local observables. For instance, the Lyapunov exponents, as done in a simpler model in [20], and in 2D NSE, [2, 24], where equivalence of the local Lyapunov spectra [41] is observed in several cases, in spite of its non local nature. Further numerical investigations by increasing both the cut-off N, and the runs duration would be extremely useful to better elucidate the equivalence between the two ensembles in the asymptotic limit when $N \to \infty$ first and $\nu \to 0$ later, the so called fully developed turbulence.

ACKNOWLEDGMENTS

This work was supported by the European Research Council (ERC) under the European Union's Horizon 2020 research and innovation programme (Grant Agreement No. 882340). VL acknowledges the support re-

ceived from the EPSRC project EP/T018178/1 and from the EU Horizon 2020 project TiPES (grant no. 820970). GM is grateful to Fabio Bonaccorso, Michele Buzzicotti and Mateo Lulli for useful discussions. This work has benefited from computational resources provided by the INFN-CINECA high performance computing facilities, by the NewTURB academic cluster at the University of Rome "Tor Vergata", and, to a smaller extent, from INFN-FARM cluster at University of Rome "La Sapienza".

Appendix A: Bound on α

We recall Eq. (4), for which it is well known, that it leads to the *a priori* bounds

$$\begin{aligned} &||\boldsymbol{u}^N(t)||_2^2 \le \max(E_0,(F_0\nu^{-1})^2) \stackrel{def}{=} \mathcal{E} \\ &\int_0^t d\tau ||\boldsymbol{\partial u}^N(\tau)||_2^2 \le \left(\frac{1}{2}\mathcal{E} + t\sqrt{F_0 E_0}\right)\nu^{-1} \end{aligned} \tag{A1}$$

satisfied (for all N) by the solution $\boldsymbol{u}$ in terms of the square L_2 norms $E_0 = ||\boldsymbol{u}(0)||_2^2 = \sum_{\beta,\boldsymbol{k}} |u_{\beta,\boldsymbol{k}}|^2 = \frac{1}{(2\pi)^3}\int |u(\boldsymbol{x})|^2 d\boldsymbol{x}$ and $F_0 = ||\boldsymbol{f}||_2$, see for instance Proposition 1, Sec.3.2 in [38]. There is no problem about the forcing term $W(\boldsymbol{u}) = \int \Delta \boldsymbol{f}\cdot\boldsymbol{u}\, d\boldsymbol{x}$ in Eq. (7) as Eq. (A1) implies, if $\Gamma = \int (\Delta \boldsymbol{u})^2\, d\boldsymbol{x} \ge D$, a bound on it: $K^2 F\sqrt{\mathcal{E}}\Gamma^{-1} \le C D^{-\frac{1}{2}}$. The other term has in the numerator $\Lambda(\boldsymbol{u}) = -\int (\boldsymbol{u}\cdot\boldsymbol{\partial u})\cdot\Delta\boldsymbol{u}\, d\boldsymbol{x}$ which is bounded via the Hölder inequality with exponents $4,4,2$ by

$$|\Lambda(\boldsymbol{u})| \le \left(\int ||\boldsymbol{u}||_2^4\, d\boldsymbol{x}\right)^{\frac{1}{4}}\left(\int ||\boldsymbol{\partial u}||_2^4\, d\boldsymbol{x}\right)^{\frac{1}{4}}\left(\int ||\Delta\boldsymbol{u}||_2^2\, d\boldsymbol{x}\right)^{\frac{1}{2}} \tag{A2}$$

and the three factors can be bounded via Sobolev's inequality [37, 42]: if $2\le q\le 6,\ a = \frac{3}{4}(q-2)$ then

$$\begin{aligned} \int_{B_r} ||\boldsymbol{u}||_2^q\, d\boldsymbol{x} \le & C_q^S\Big[\left(\int_{B_r} ||\boldsymbol{\partial u}||_2^2\, d\boldsymbol{x}\right)^a \cdot \left(\int_{B_r} ||\boldsymbol{u}||_2^2\, d\boldsymbol{x}\right)^{q/2-a} + \\ & + r^{-2a}\left(\int_{B_r} ||\boldsymbol{u}||_2^2\, d\boldsymbol{x}\right)^{q/2}\Big] \end{aligned} \tag{A3}$$

where B_r is a sphere of radius r and the integrals are performed with respect to $d\boldsymbol{x}$. The C_q^S is a suitable constant. The second term of the right hand side can be omitted if $\boldsymbol{u}$ has zero average over B_r.

Therefore in the above case, where $\boldsymbol{u}, \boldsymbol{\partial u}, \Delta\boldsymbol{u}$ do have zero average, choose $q=4, a=\frac{3}{2}$, $B_r = [0,2\pi]^3$; calling $\overline{C}_4^S = (C_4^S)^{\frac{1}{4}}$ and $\Gamma = \int(\Delta\boldsymbol{u})^2\, d\boldsymbol{x}$, it is:

$$\Lambda(\boldsymbol{u}) \le \overline{C}_4^S(\mathcal{E}^{\frac{1}{8}}D^{\frac{3}{8}})\,\overline{C}_4^S(D^{\frac{1}{8}}\Gamma^{\frac{3}{8}})\Gamma^{\frac{1}{2}} \le \overline{C}\mathcal{E}^{\frac{1}{8}}D^{\frac{1}{2}}\Gamma^{\frac{7}{8}} \tag{A4}$$

so that

$$\begin{aligned} |\alpha(\boldsymbol{u})| \le & C_1(\mathcal{E}^{\frac{1}{8}}D^{\frac{1}{2}}\Gamma^{-\frac{1}{8}} + \mathcal{E}^{\frac{1}{2}}\Gamma^{-1}) \\ \le & C(\mathcal{E}^{\frac{1}{8}}D^{\frac{3}{8}} + \mathcal{E}^{\frac{1}{2}}D^{-1}) < C_2(\sqrt{D} + \sqrt{D}^{-1}) \end{aligned} \tag{A5}$$

and $|\alpha(\boldsymbol{u}(t))|$ is thus bounded, for any solution and any N, by a constant: $|\alpha| \le \kappa$.

Appendix B: Reversible Navier Stokes global smoothness

Let $\varepsilon < \alpha(\boldsymbol{u}(t)) \le \kappa$ and suppose that the initial data $\boldsymbol{u}(0)$ and $\boldsymbol{f}$ satisfy $||\boldsymbol{u_k}||_2, ||\boldsymbol{f_k}||_2 < c_p k^{-p}$ for all $p>0$ (recall that we consider only initial data and force with a finite number, $\le N$, of modes, for simplicity). Let $a(t,\tau) = \int_\tau^t \alpha(\boldsymbol{u}(t')dt'$; then $\varepsilon(t-\tau) < a(t,\tau) < \kappa(t-\tau)$.

Following, for instance, [38], we can write $\boldsymbol{u_k}(t) = e^{-a(t,0)k^2}\boldsymbol{u_k}(0) + \int_0^t e^{-a(t,\tau)k^2}(\mathrm{N}_{\boldsymbol{k}}(\boldsymbol{u}(\tau)) + \boldsymbol{f_k})d\tau$, where $\mathrm{N}_{\boldsymbol{k}}(\boldsymbol{u}(\tau))$ is the non-linear term of the NSE. Therefore, the sum of the first and last term can be bounded by $\frac{2c_p}{k^p}$ while the integral is bounded by

$$\begin{aligned} &\int_0^t e^{-\varepsilon k^2(t-\tau)} \sum_{\boldsymbol{p}+\boldsymbol{q}=\boldsymbol{k}} ||\boldsymbol{u_p}\cdot\boldsymbol{q}||_2 ||\boldsymbol{u_q}||_2\, d\tau \\ &\le \frac{\sqrt{\mathcal{E}}\sqrt{D}(1-e^{-\varepsilon k^2 t})}{\varepsilon k^2} \end{aligned} \tag{B1}$$

so that adding the two bounds: $||\boldsymbol{u_k}||_2^2 < \frac{C_2}{k^2}$ for a suitable C_2. Therefore, again, $||\boldsymbol{u_k}(t)||_2$ can be bounded by adding $\frac{2c_p}{k^p}$ and a bound on

$$\int_0^t e^{-\varepsilon k^2(t-\tau)} \sum_{\boldsymbol{p}+\boldsymbol{q}=\boldsymbol{k}} \frac{||\boldsymbol{p}||_2||\boldsymbol{u_p}||_2\, ||\boldsymbol{q}||_2^2||\boldsymbol{u_q}||_2}{||\boldsymbol{p}||_2||\boldsymbol{q}||_2}\, d\tau \tag{B2}$$

A bound on the latter integral is obtained via the Schwartz inequality and the remark that $\boldsymbol{p}+\boldsymbol{q}=\boldsymbol{k}$ implies $||\boldsymbol{p}||_2||\boldsymbol{q}||_2 \ge \frac{k_0}{2}||\boldsymbol{k}||_2, k_0 = 1$, and

$$\begin{aligned} &\sum_{\boldsymbol{p}+\boldsymbol{q}=\boldsymbol{k}} \frac{||\boldsymbol{p}||_2||\boldsymbol{u_p}||_2||\boldsymbol{q}||_2^2||\boldsymbol{u_q}||_2}{||\boldsymbol{p}||_2||\boldsymbol{q}||_2} \le \frac{2C_2}{k_0}\sum_{\boldsymbol{p}+\boldsymbol{q}=\boldsymbol{k}} \frac{||\boldsymbol{p}||_2||\boldsymbol{u_p}||_2}{||\boldsymbol{p}||_2||\boldsymbol{q}||_2} \\ &\le \frac{2C_2}{k_0}\sqrt{D}\left(\sum_{\boldsymbol{p}+\boldsymbol{q}=\boldsymbol{k}} \frac{1}{(||\boldsymbol{p}||_2||\boldsymbol{q}||_2)^2}\right)^{\frac{1}{2}} \\ &\le \left(\frac{2C_2}{k_0}\right)^{1+\frac{1}{8}} ||\boldsymbol{k}||_2^{-\frac{1}{4}}\sqrt{D}\left(\sum_{\boldsymbol{p}+\boldsymbol{q}=\boldsymbol{k}} \frac{1}{(||\boldsymbol{p}||_2||\boldsymbol{q}||_2)^{2-\frac{1}{4}}}\right)^{\frac{1}{2}} \\ &\le \left(\frac{2C_2}{k_0}\right)^{1+\frac{1}{8}} \sqrt{D}||\boldsymbol{k}||_2^{-\frac{1}{4}}\left(\sum_{\mathbf{n}} \frac{1}{||\mathbf{n}||_2^{4-\frac{1}{2}}}\right)^{\frac{1}{2}} \end{aligned} \tag{B3}$$

where $\boldsymbol{p}$ has been changed to $\mathbf{n}$ just to make clear that summing over $\boldsymbol{p}+\boldsymbol{q}=\boldsymbol{k}$ allows using the Schwartz inequality. Hence integration over t, as in Eq. (B1), yields

$$||\boldsymbol{u_k}(t)||_2 \le \frac{\gamma_1}{k^{2+\frac{1}{4}}} \tag{B4}$$

Thus if D is finite the bound $||\boldsymbol{u_k}||_2 < \gamma k^{-2}$, Eq. (B1), can be improved into $||\boldsymbol{u_k}||_2 < \gamma_1 k^{-2-\frac{1}{4}}$. Iterating a

autoregularization phenomenon sets in and

$$||\boldsymbol{u}_{\boldsymbol{k}}(t)||_2 \leq \frac{\gamma_p}{k^{2+\frac{1}{4}p}} \qquad \text{for all } p \geq 1 \tag{B5}$$

so that $\boldsymbol{u}(t)$ is a C^∞-functions and all its derivatives can be bounded in terms of the enstrophy D, uniformly in N. See Sec. 3.3 in [38] for related results on the classic autoregularization.

Appendix C: Numerical parameters

Table I summarizes the values of various observables corresponding to the runs with different kinematic viscosities and cut-offs. The parentheses present the statistical error of the last digit in a given value. We define the following: physical length of the container $L = 2\pi$, root-mean-square velocity $u_{\rm rms} = \sqrt{\langle||\boldsymbol{u}||_2^2\rangle/3}$, averaged rate of energy dissipation $\varepsilon = \nu\,\langle D\rangle$, $k_\nu = \left(\frac{\varepsilon}{\nu^3}\right)^{1/4}$ is the Kolmogorov scale, Taylor length $\lambda = u_{\rm rms}\sqrt{\frac{15}{\langle D\rangle}}$, integral length $\ell = \frac{3L}{8}\langle\sum_{\boldsymbol{k}} k^{-1}E(\boldsymbol{k})/\sum_{\boldsymbol{k}} E(\boldsymbol{k})\rangle$ (see Eq. 13), Taylor-Reynolds number $\mathrm{Re}_\lambda = \frac{u_{\rm rms}\lambda}{\nu}$, Reynolds number $\mathrm{Re} = \frac{u_{\rm rms}\ell}{\nu}$, large-eddy turnover time $T_\ell = \frac{\ell}{u_{\rm rms}}$.

We present the final $D/\mathcal{D}$ ratio, which is an abbreviation for $D/\mathcal{D} \equiv D/\langle\mathcal{D}(\boldsymbol{u})\rangle_\nu^{\mathcal{I},N}$. Ideally, this should be 1, and it is indeed unity when we start the $\mathcal{R}$ simulation based on the ensemble average $\langle\mathcal{D}(\boldsymbol{u})\rangle_\nu^{\mathcal{I},N}$ from $\mathcal{I}$. But for almost all runs, we increased the statistics of $\mathcal{I}$, which eventually improved $\langle\mathcal{D}(\boldsymbol{u})\rangle_\nu^{\mathcal{I},N}$. Therefore the $D/\mathcal{D}$ ratio gives an estimate of the quality of each collection $\mathcal{E}^{\mathcal{R},N}$ of $\mathcal{R}$ runs with respect to the collection $\mathcal{E}^{\mathcal{I},N}$ for a particular ν. A significant $D/\mathcal{D}$ discrepancy would also explain possible discrepancies in $\langle\alpha\rangle/\nu$ and accordingly other ratios of observables.

The ratio T/T_ℓ, where T is the total length of the simulation in physical units, is essentially an indicator of the statistical significance of the generated ensemble. Empty entries (filled with a "–") are met in cases at the quasi-thermalized regime for particular observables of which the definitions are relevant in the hydrodynamic regime (e.g. k_ν, λ).

An interesting fact about Table I is that the averaged values for each entry turn out to be the same on average, up to statistical errors, for both $\mathcal{R}$ and $\mathcal{I}$. Showing one value, implies that is it the same for $\mathcal{R}$ and $\mathcal{I}$ at the particular N_0 and ν. When the averages are not the same within statistical errors we show both estimates in the form $\mathcal{R}|\mathcal{I}$. This happened in the case of $N_0 = 256$ in two cases, namely R11◯ and R15□, see e.g. ε. For R11◯ we attribute this to poor statistics, notice $T/T_\ell = 374$, which is the lowest, and for R15□ we attribute to a poor estimation of $\langle\mathcal{D}(\boldsymbol{u})\rangle_\nu^{\mathcal{I},N}$, notice $D/\mathcal{D} = 1.034(2)$, which is the highest.

[1] G. Gallavotti, *Nonequilibrium and irreversibility*, Theoretical and Mathematical Physics (Springer-Verlag, 2014).
[2] G. Gallavotti, Journal of Statistical Physics **180**, 172 (2020).
[3] U. Frisch, *Turbulence: The Legacy of A. N. Kolmogorov* (Cambridge University Press, 1995).
[4] S. B. Pope, *Turbulent Flows* (Cambridge University Press, 2000).
[5] R. Salmon, *Lectures on geophysical fluid dynamics* (Oxford University Press, 1998).
[6] A. Alexakis and L. Biferale, Physics Reports **767**, 1 (2018).
[7] U. Frisch, S. Kurien, R. Pandit, W. Pauls, S. S. Ray, A. Wirth, and J.-Z. Zhu, Phys. Rev. Lett. **101**, 144501 (2008).
[8] C. Cercignani, "The boltzmann equation," in *The Boltzmann Equation and Its Applications* (Springer New York, New York, NY, 1988) pp. 40–103.
[9] R. Zwanzig, *Nonequilibrium statistical mechanics* (Oxford university press, 2001).
[10] L. Onsager and S. Machlup, Phys. Rev. **91**, 1505 (1953).
[11] L. Bertini, A. De Sole, D. Gabrielli, G. Jona-Lasinio, and C. Landim, Journal of Statistical Physics **107**, 635 (2002).
[12] D. Ruelle, *Statistical Mechanics* (CO-PUBLISHED WITH IMPERIAL COLLEGE PRESS, 1999) https://www.worldscientific.com/doi/pdf/10.1142/4090.
[13] H. Touchette, Journal of Statistical Physics **159**, 987 (2015).
[14] D. J. Evans and G. P. Morriss, *Statistical Mechanics of Nonequilibrium Fluids* (Academic Press, New-York, 1990).
[15] Z. She and E. Jackson, Physical Review Letters **70**, 1255 (1993).
[16] G. Gallavotti, Physics Letters A **223**, 91 (1996).
[17] G. Gallavotti, Physica D **105**, 163 (1997).
[18] G. Gallavotti, L. Rondoni, and E. Segre, Physica D **187**, 358 (2004).
[19] G. Gallavotti, European Physics Journal, E **43:37** (2020), 10.1140/epje/i2020-11961-0.
[20] G. Gallavotti and V. Lucarini, Journal of Statistical Physics **156**, 1027 (2014).
[21] L. Biferale, M. Cencini, M. D. Pietro, G. Gallavotti, and V. Lucarini, Physical Review E **98**, 012201 (2018).
[22] M. D. Pietro, L. Biferale, G. Boffetta, and M. Cencini, The European Physical Journal E **41**, 48 (2018).
[23] K. Seshasayanan, K. S. Eswaran, M. Maji, S. Ghosh, and V. Shukla, "Equivalence of nonequilibrium ensembles: Two-dimensional turbulence with a dual cascade," (2021), arXiv:2112.12215 [physics.flu-dyn].
[24] G. Gallavotti, European Physics Journal Special Topics **227**, 217 (2018).
[25] G. Gallavotti, Springer Proceedings in Mathematics & Statistics **282**, 569 (2019).
[26] G. Gallavotti, Journal of Statistical Physics **185** (2021), 10.1007/s10955-021-02830-1.
[27] V. Shukla, B. Dubrulle, S. Nazarenko, G. Krstulovic, and

TABLE I. Values of various observables corresponding to the numerical simulations, labeled as R# indicating the run numbering, with different kinematic viscosities and cut-offs. All resulting parameters are the same up to statistical errors (which are included inside the parentheses for the error of the last digit) for both $\mathcal{I}$ and $\mathcal{R}$, except for those cases separated as $\mathcal{R}|\mathcal{I}$. $D/\mathcal{D}$ is an abbreviation for $D/\mathcal{D} \equiv D/\langle \mathcal{D}(\boldsymbol{u})\rangle_\nu^{\mathcal{I},N}$. The symbols next to the Run numbering correspond to the statistical regimes; ◯: Hydrodynamic, △: Crossover, □: Quasi-thermalized.

$N_0 = 64$	R1◯	R2◯	R3△	R4□	R5□
ν	5×10^{-2}	10^{-2}	10^{-3}	10^{-4}	10^{-5}
$\langle\alpha\rangle/\nu$	1.015(7)	0.999(3)	1.000(4)	1.000(8)	0.93(20)
$D/\mathcal{D}$	0.998(2)	0.999(1)	0.999(1)	1.000(1)	1.01(2)
$u_{\rm rms}$	1.22(1)	1.30(1)	1.46(1)	2.92(1)	7.00(1)
Re	43	185	1705	7.9×10^3	1.2×10^5
Re_λ	30	77	300	–	–
ε	0.74	0.72	0.76	0.66	0.39
k_ν	8	29	165	–	–
λ	1.23	0.59	0.21	–	–
ℓ	1.77	1.43	1.16	0.27	0.17
T/T_ℓ	8300	1.3×10^4	2.3×10^4	1.8×10^5	5.8×10^5

$N_0 = 128$	R6◯	R7◯	R8△	R9△	R10□
ν	5×10^{-2}	10^{-2}	10^{-3}	10^{-4}	10^{-5}
$\langle\alpha\rangle/\nu$	1.01(3)	0.995(5)	1.011(6)	0.99(1)	0.99(2)
$D/\mathcal{D}$	1.008(2)	0.998(1)	0.996(2)	0.999(2)	1.027(1)
$u_{\rm rms}$	1.22(4)	1.29(3)	1.36(3)	1.88(4)	4.61(1)
Re	43	183	1850	1.4×10^4	6.1×10^4
Re_λ	30	76	267	1570	–
ε	0.75	0.71	0.73	0.76	0.68
k_ν	8	29	164	932	–
λ	1.22	0.59	0.20	0.08	–
ℓ	1.78	1.42	1.36	0.72	0.13
T/T_ℓ	760	4690	4950	10^4	1.1×10^5

$N_0 = 256$	R11◯	R12◯	R13△	R14△	R15□
ν	5×10^{-2}	10^{-2}	10^{-3}	10^{-4}	10^{-5}
$\langle\alpha\rangle/\nu$	1.06(4)	0.99(2)	1.00(2)	1.00(2)	0.94(2)
$D/\mathcal{D}$	1.008(2)	1.008(1)	1.008(2)	1.019(2)	1.034(2)
$u_{\rm rms}$	1.25|1.21	1.29(5)	1.35(5)	1.46(5)	2.70(6)
Re	44	184	1800	1.7×10^4	10^5
Re_λ	31	76	260	973	–
ε	0.78|0.73	0.71	0.73	0.71	0.74|0.79
k_ν	8	29	164	919	–
λ	1.26|1.22	0.59	0.19	0.06	–
ℓ	1.80	1.42	1.33	1.18	0.36
T/T_ℓ	374	680	760	800	3950

R16◯	ν	$\langle\alpha\rangle/\nu$	$D/\mathcal{D}$	$u_{\rm rms}$	Re	Re_λ
	10^{-3}	0.97(3)	0.997(2)	1.35(5)	1800	260
$N_0 = 512$	ε	k_ν	λ	ℓ	T/T_ℓ	
	0.71(7)	163	0.19	1.35	400	

S. Thalabard, Phys. Rev. E **100**, 043104 (2019).

[28] A. Jaccod and S. Chibbaro, Phys. Rev. Lett. **127**, 194501 (2021).

[29] C. Fefferman, *Existence & smoothness of the Navier–Stokes equation*, The millennium prize problems (Clay Mathematics Institute, Cambridge, MA, 2000) pp. 57–67.

[30] J. C. Maxwell, *The Scientific Papers of James Clerk Maxwell*, edited by W. D. Niven, Cambridge Library Collection - Physical Sciences, Vol. 2 (Cambridge University Press, 2011).

[31] G. Gallavotti, Chaos **16**, 043114 (+6) (2006).

[32] A. Alexakis and M. Brachet, Journal of Fluid Mechanics **884**, A33 (2020).

[33] S. A. Orszag, Journal of the Atmospheric sciences **28**, 1074 (1971).

[34] D. Pekurovsky, SIAM Journal on Scientific Computing **34**, C192 (2012), https://doi.org/10.1137/11082748X.

[35] C. Brun and A. Pumir, Phys. Rev. E **63**, 056313 (2001).

[36] J. Leray, Acta Mathematica **63**, 193 (1934).

[37] L. Caffarelli, R. Kohn, and L. Nirenberg, Communications on Pure and Applied Mathematics **35**, 771 (1982).

[38] G. Gallavotti, *Foundations of Fluid Dynamics* ((second printing) Springer Verlag, Berlin, 2005).

[39] J.Serrin, Archive for Rational Mechanics and Analysis **9**, 187 (1962).

[40] R. H. Kraichnan, Advances in Mathematics **16**, 305 (1975).

[41] Obtained from the Jacobian matrix, formally $J(\boldsymbol{u}) = \frac{\partial \dot{\boldsymbol{u}}}{\partial \boldsymbol{u}}$, by averaging over time the spectrum $\lambda_0(\boldsymbol{u})$, $\lambda_1(\boldsymbol{u})$, ..., of the symmetric part of $J(u)$.

[42] S. Sobolev, *Applications of Functional analysis in Mathematical Physics*, Translations of the American Mathematical Society, Vol. 7 (AMS, Providence, 1963).